

1 **Technical Note: Evaluation of simultaneous measurements of mesospheric OH, HO₂, and O₃**
2 **under photochemical equilibrium assumption: Statistical approach**

3
4 Mikhail Yu. Kulikov¹, Anton A. Nechaev¹, Mikhail V. Belikovich¹, Tatiana S. Ermakova¹, and
5 Alexander M. Feigin¹

6
7 ¹Institute of Applied Physics of the Russian Academy of Sciences, 46 Ulyanov Str., 603950 Nizhny
8 Novgorod, Russia

9
10 Correspondence to: Mikhail Yu. Kulikov (mikhail_kulikov@mail.ru)

11
12 **Abstract**

13
14 The Technical Note presents a statistical approach to evaluating simultaneous measurements of
15 several atmospheric components under the assumption of photochemical equilibrium. We consider
16 simultaneous measurements of OH, HO₂, and O₃ at the altitudes of the mesosphere as a specific
17 example and their daytime photochemical equilibrium as an evaluating relationship. A simplified
18 algebraic equation relating local concentrations of these components in the 50-100 km altitude
19 range has been derived. The parameters of the equation are temperature, neutral density, local
20 zenith angle, and the rates of 8 reactions. We have performed a one-year simulation of the
21 mesosphere and lower thermosphere using a 3D chemical-transport model. The simulation shows
22 that the discrepancy between the calculated evolution of the components and the equilibrium value
23 given by the equation does not exceed 3-4% in the full range of altitudes independent of season or
24 latitude. We have developed the technique of statistic Bayesian evaluation of simultaneous
25 measurements of OH, HO₂ and O₃ based on the equilibrium equation taking into account the
26 measurement error. The first results of application of the technique to MLS/Aura data are
27 presented in this Technical Note. It has been found that the satellite data of HO₂ distribution
28 regularly demonstrates essentially lower altitudes of mesospheric maximum of this component.
29 This has also been confirmed by model HO₂ distributions and comparison with offline retrieval of
30 HO₂ from the daily zonal means MLS radiance.

1. Introduction

A prominent feature of the atmospheric photochemical systems is the presence of a large number of chemical components with short lifetime and concentrations close to stable photochemical equilibrium at every instant. The condition of balance between their sources and sinks is described by a system of algebraic equations. This system can be used to determine characteristics of hard to measure atmospheric species through other measurable components, evaluate results of remote or *in situ* measurements, estimate reaction rates usually known with significant uncertainty, and to understand processes and chemical reactions that influence variability of the most important atmospheric components, e.g. ozone, in the geographical region of interest.

This approach has found wide application:

(1) in 3D chemical transport models that include a large set of physical and chemical processes with a broad spectrum of spatio-temporal scales. In particular, the chemical family concept is widely used for simulating gas phase photochemistry of the lower and middle atmosphere (e.g., Douglass et al., 1989; Kaye and Rood, 1989; Rasch et al., 1995), when transport is taken into account only for the concentration of a chemical family, while relative concentrations of the constituent fast components are calculated from the instantaneous stable equilibrium condition. Complemented with the Henry law (e.g., Djouad et al., 2003; Tulet et al., 2006) in multiphase models, this approach markedly saves calculation time and increases the overall stability of the numerical scheme. Moreover, the use of the photochemical equilibrium condition to simulate fast components dynamics reduces the phase space dimension of box models significantly (e.g., Kulikov and Feigin, 2014), allowing a comprehensive analysis of nontrivial nonlinear dynamic properties of various atmospheric photochemical systems (e.g., Feigin and Konovalov, 1996; Feigin et al., 1998; Konovalov et al., 1999; Konovalov and Feigin, 2000; Kulikov et al., 2012).

(2) in investigations of the chemistry of the surface layer and free troposphere in different regions (over megalopolises, in rural areas, in the mountains, over the seas) based on measurements of nitrogen species, peroxy radicals, ozone, aerosols, and other components aimed at understanding processes impacting the surface ozone formation and air quality. The equilibrium condition is most frequently used for nitrogen species. For example, Chameides (1975) proposed a model for determining the vertical distribution of odd nitrogen, in which the HNO_3 profile could be

63 deployed to retrieve profiles of five other components (NO, NO₂, NO₃, N₂O₅, and HNO₂) from their
64 photochemical equilibrium condition. In the paper by Stedman et al. (1975) the equation for NO₂
65 equilibrium that accounted only for the main source and sink of this component was applied to
66 determine the photodissociation constant J(NO₂). A more accurate equation for the NO₂ equilibrium
67 was used by Crawford et al. (1996) and Kondo et al. (1996) to determine the NO₂/NO partitioning
68 and NO_x, allowing, in particular, investigating the spatial distribution of NO_x/NO_y over the Pacific.

69 Night-time equilibrium in the NO₂-NO₃-N₂O₅ system is used to determine surface layer N₂O₅
70 concentration, equilibrium constant of this system, equilibrium partitioning between NO₃ and N₂O₅,
71 and loss coefficients of NO₃, N₂O₅ and NO_x (Martinez et al., 2000; Brown et al., 2003; Crowley et
72 al., 2010; McLaren et al., 2010; Benton et al., 2010; Sobanski et al., 2016).

73 Platt et al. (1979) used the CH₂O photochemical equilibrium condition to analyse results of
74 simultaneous measurement of CH₂O, O₃ and NO₂ and to identify mechanisms of CH₂O formation
75 over rural areas and in maritime air. In the papers by Ko et al. (2003), Cantrell et al. (2003),
76 Penkett et al. (1997), Penkett et al. (1998) algebraic expressions derived from equilibrium
77 conditions for H₂O₂, peroxy radicals and nitrogen species were used to determine equilibrium
78 values of peroxide concentration, total peroxy radical level, and NO/NO₂ ratio, and to diagnose the
79 ozone production and loss levels in clean or polluted troposphere.

80 (3) in stratospheric chemistry studies, including determination of a critical parameter in
81 catalytic cycles of ozone destruction in the polar stratosphere. In particular, the equilibrium
82 condition for ClO and Cl₂O₂ along with the measurement data of daytime and night-time
83 concentrations of these components in the polar stratosphere are used to evaluate the temperature
84 dependence of the ClO concentration, reaction constants determining the
85 ClO + ClO + M ↔ Cl₂O₂ + M equilibrium, and the photolysis rate of Cl₂O₂ (Ghosh et al., 1997;
86 Avallone et al., 2001, Solomon et al., 2002; Stimpfle et al., 2004; von Hobe et al., 2005; Berthet et
87 al., 2005; Butz et al., 2007; von Hobe et al., 2007; Kremser et al., 2011; Sumińska-Ebersoldt et al.,
88 2012; Wetzel et al., 2012).

89 Pyle et al. (1983) proposed a method for derivation of the OH concentration from satellite
90 infrared measurements of NO₂ and HNO₃ using a simple algebraic relation following from the
91 equilibrium condition for HNO₃. Algorithms for retrieving distributions of OH and HO₂ from the
92 satellite measurement data of O₃, NO₂, H₂O, HNO₃ by LIMS/Nimbus 7 and UARS with the help of
93 algebraic models following from the photochemical equilibrium of O_x, HO_x and HNO₃ components

94 were proposed by Pyle and Zavody (1985), Pickett and Peterson (1996). It is also worthy of note
95 that similar models are widely used for calculating concentrations of components with a short
96 lifetime (e.g. O(¹D) and OH) and subsequent evaluating vertical distributions of eddy diffusivity from
97 measurements of trace gas concentration profiles (see, e.g., Massie and Hunten, 1981).

98 Kondo et al. (1988) made use of the photochemical equilibrium between NO and NO₂ for
99 understanding diurnal variations of NO concentration measured during aircraft flights. In the paper
100 by Webster et al. (1990) simultaneous *in situ* balloon-borne measurements of NO, NO₂, HNO₃, O₃
101 and N₂O and the photochemical equilibrium condition for various nitrogen components were used
102 to determine OH, N₂O₅ and NO_y concentrations. A similar approach was employed by Kawa et al.
103 (1990), who obtained NO₂, N₂O₅, ClNO₃, HNO₃ and OH concentrations from aircraft measurements
104 of NO, ClO and O₃ concentrations. Hauchecorne et al. (2010) found that NO₃ concentration
105 measured by GOMOS/ENVISAT positively correlates with temperature at altitudes up to 45 km in
106 the region where NO₃ is in chemical equilibrium with O₃. Funke et al. (2005) used NO and NO₂
107 stable-state photochemistry to verify correctness of the new approach of retrieving distributions of
108 those component from MIPAS/ENVISAT measurement data. Marchand et al. (2007) proposed a
109 method to retrieve the temperature distribution in the stratosphere between 30 km and 40 km from
110 O₃ and NO₃ measurements by GOMOS with the help of a simple equation derived from the night-
111 time NO₃ chemical equilibrium.

112 (4) in investigations of the chemistry of O_x-HO_x components and atmospheric glows in the
113 mesosphere and MLT area. In particular, Kulikov et al. (2006, 2009) proposed algorithms for the
114 simultaneous retrieval of O, H, HO₂ and H₂O from joint OH and O₃ satellite measurement, in which
115 the assumption of photochemical equilibrium of O₃, OH, and HO₂ was utilized. For several decades
116 the assumption of the photochemical equilibrium of ozone (PEO) was widely used to determine
117 distributions of atomic oxygen and atomic hydrogen at altitudes of the MLT via satellite and rocket
118 measurement of ozone concentration and airglow emissions (e.g., Evans and Llewellyn, 1973;
119 Good, 1976; Pendleton et al., 1983; McDade et al., 1985; McDade and Llewellyn, 1988; Evans et
120 al., 1988; Thomas, 1990; Llewellyn et al., 1993; Llewellyn and McDade, 1996; Mlynczak et al.,
121 2007, 2013a, 2013b, 2014; Smith et al., 2010; Siskind et al., 2008, 2015). Russell and Lowe (2003)
122 applied PEO to infer the seasonal and global climatology of atomic oxygen using WINDII/UARS.
123 PEO was deployed to investigate hydroxyl emission mechanisms, morphology, and variability in
124 the upper mesosphere – lower thermosphere region (Marsh et al., 2006; Xu et al., 2010, 2012;

125 Kowalewski et al., 2014). Mlynczak and Solomon (1991, 1993) and Mlynczak et al. (2013b) used
126 the equilibrium assumption to derive exothermic chemical heat. The PEO assumption employed for
127 studying the mesospheric OH* layer response to gravity waves (Swenson and Gardner, 1998). In
128 ultimately theoretical works, e.g. Grygalashvyly et al. (2014), Grygalashvyly (2015), PEO was used
129 to derive the dependence of excited hydroxyl layer concentration and altitude on atomic oxygen
130 and temperature. In the paper by Sonnemann et al. (2015) it was used to analyze annual variations
131 of OH* layer. Moreover, PEO is frequently applied implicitly, when authors are equating the night-
132 time loss of ozone in the reaction with atomic hydrogen and production of ozone by a 3-body
133 reaction of molecular and atomic oxygen (e.g., Nikoukar et al., 2007).

134 In the present Technical note we demonstrate how the photochemical equilibrium condition
135 of several atmospheric components may be employed to statistically validate data of their
136 simultaneous measurements, particularly in the case when measurement error is large.

137 We consider the simultaneous photochemical daytime equilibrium of OH, HO₂, and O₃ at the
138 altitudes of the mesosphere. We have derived a simplified algebraic equation

$$139 \quad F(OH, HO_2, O_3) = 1,$$

140 describing the relationship between local concentrations of the components at the altitudes of 50–
141 100 km. The only parameters of the equation are temperature, neutral density, local zenith angle,
142 and constants of 8 reactions. One-year simulation of the mesosphere and lower thermosphere
143 based on a 3D chemical-transport model shows that the discrepancy between the calculated
144 evolution of the components and the equilibrium value given by the equation does not exceed 3–
145 4 % in the full range of altitudes independent of season or latitude.

146 We have developed a technique of statistical Bayesian evaluation of simultaneous
147 measurement of OH, HO₂ and O₃ based on the mentioned equilibrium equation taking into account
148 the measurement error. The first results of its application to MLS/Aura data (Wang et al., 2015a,b;
149 Schwartz et al., 2015) are presented. It is found that the satellite data of HO₂ distribution regularly
150 demonstrates essentially lower altitudes of this component's mesospheric maximum. These results
151 confirm the ones obtained via the offline retrieval of HO₂ from the MLS primary data (Millán et al.,
152 2015).

153 The Technical Note is structured as follows. A 3D chemical transport model is briefly
154 described in Sect. 2. In Sect. 3 a simplified algebraic relationship between the equilibrium
155 concentrations of OH, HO₂ and O₃ is derived and verified by 3D simulations. Section 4 presents the

156 method of statistical evaluation of simultaneous data of OH, HO₂ and O₃. The results of applying
157 the method to MLS/Aura data are presented in Sect. 5. The last Section contains discussion of the
158 results followed by concluding remarks.

160 **2. Model and calculations**

161
162 For our calculations we used the global 3D chemical transport model (CTM) of the middle
163 atmosphere developed by the Leibniz Institute of Atmospheric Physics (IAP) (e.g., Berger, 1994;
164 Ebel et al., 1995; Sonnemann et al., 1998; Kremp et al., 1999; Berger and von Zahn, 1999;
165 Hartogh et al., 2004, 2011; Sonnemann et al., 2006, 2007). It was designed particularly for
166 investigation of the spatio-temporal structure of phenomena in the MLT region and specifically in
167 the extended mesopause region. The grid-point model extends from the ground up to the middle
168 thermosphere (0–150 km; 118 pressure-height levels). The horizontal resolution amounts to 5.625°
169 latitudinally and 5.625° longitudinally. The chemical module described in numerous papers (e.g.,
170 Sonnemann et al., 1998; Körner and Sonnemann, 2001; Grygalashvyly et al., 2009, 2011, 2012)
171 consists of 19 constituents, 49 chemical reactions, and 14 photo-dissociation reactions (see Table
172 1). The reaction rates used in the model are taken from Burkholder et al. (2015). The temperature-
173 dependent reaction rates are calculated on-line, thus, they are sensitive to small temperature
174 fluctuations. We make use of the pre-calculated dissociation rates (Kremp et al., 1999).

175 The evolution of the components of HO_x (H, OH, HO₂, H₂O₂) and NO_x (N, NO, NO₂, NO₃)
176 families is calculated using the chemical family concept proposed by Shimazaki (Shimazaki, 1985).
177 This is done because of the presence of short-lived components among these families, with
178 lifetimes much shorter than those of the families themselves, which imposes significant restrictions
179 on the value of the CTM's integration step. For example, the daytime lifetimes of OH and HO₂
180 above 70 km are about 1 s or less, while the lifetime of the HO_x family is about 10⁴ s or more.
181 Therefore, when calculating these components individually it is necessary to set the CTM's
182 integration step to be much less than 1 s. In our work, the Shimazaki technique is applied for
183 calculating the evolution of each component of the HO_x and NO_x families. We emphasize that this
184 technique does not explicitly use the steady-state approximation for the components, instead it
185 utilizes the approach based on an implicit Euler scheme (see Shimazaki, 1985). This allows

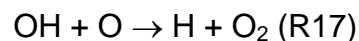
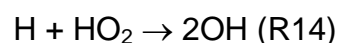
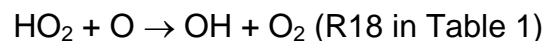
186 increasing the integration step of CTM significantly without loss of accuracy of calculating the short-
187 lived components. In our work the integration time is chosen to be 9 s.

188 The model includes 3D advective and vertical diffusive transport (turbulent and molecular).
189 Three-dimensional fields of temperature and winds are taken from the Canadian Middle
190 Atmosphere Model (CMAM) for the year 2000 (de Grandpre et al., 2000; Scinocca et al., 2008).
191 We use the Walcek-scheme (Walcek and Aleksic, 1998; Walcek, 2000) for advective transport and
192 the implicit Thomas algorithm as described in Morton and Mayers (1994) for diffusive transport.
193 The vertical eddy diffusion coefficient is based on the results by Lübken (1997).

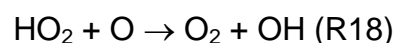
194 We calculate the annual variation of spatio-temporal distributions of OH, HO₂, and O₃ and
195 constructed distributions of the $F(OH,HO_2,O_3)$ function introduced in Sect. 1. To remove transitional
196 regions that correspond to sunset and sunrise, we take into account only periods of local time with
197 the solar zenith angle $\chi < 85^\circ$. The obtained results are presented in the model coordinates, so the
198 pressure-height levels are used for the vertical axes. In addition, the approximate altitudes are
199 shown in the figures of Sec. 1, calculated for a given month utilizing averaged temperature profiles
200 of the model and hydrostatic equilibrium.

202 **3. Daytime photochemical equilibrium of OH, HO₂, and O₃ at the altitudes of the mesosphere**

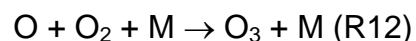
204 The daytime balance of OH concentration at mesospheric altitudes is determined by the following
205 primary reactions (Brasseur and Solomon, 2005):

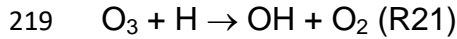
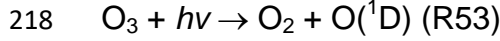
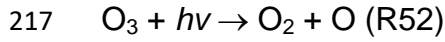


211 The daytime balance of HO₂ concentration:



215 The daytime balance of O₃ concentration:





220 Expressions for local concentrations of OH, HO₂, and O₃ in the photochemical equilibrium

221 are written in the form

222
$$OH = \frac{k_{18} \cdot HO_2 \cdot O + 2k_{14} \cdot HO_2 \cdot H + k_{21} \cdot O_3 \cdot H}{k_{17} \cdot O + k_{22} \cdot O_3}, \quad (1)$$

223
$$HO_2 = \frac{k_{20} \cdot M \cdot O_2 \cdot H + k_{22} \cdot O_3 \cdot OH}{k_{18} \cdot O}, \quad (2)$$

224
$$O_3 = \frac{k_{12} \cdot M \cdot O_2 \cdot O}{k_{52} + k_{53} + k_{21} \cdot H}, \quad (3)$$

225 where k_i are the corresponding reaction constants from Burkholder et al. (2015).

226 We eliminate O and H from Eqs. (1)-(3) and derive an expression depending only on OH, HO₂, O₃.

227 Almost everywhere in the mesosphere and lower thermosphere (with the exception of 85-95
228 km, see Kulikov et al., 2017) the photodissociation is the main ozone sink, i.e. $k_{52} + k_{53} \gg k_{21} \cdot H$.

229 Therefore, in the zero order approximation Eq. (3) can be simplified and the concentration of
230 atomic oxygen can be defined in terms of ozone concentration:

231
$$O = \frac{k_{52} + k_{53}}{k_{12} \cdot M \cdot O_2} O_3 \quad (4)$$

232 Making use of Eq. (4) we can derive from Eq. (2) an expression for the concentration of H in terms
233 of concentrations of OH, HO₂ and O₃:

234
$$H = \frac{k_{18} \cdot (k_{52} + k_{53}) / (k_{12} \cdot M \cdot O_2) \cdot HO_2 - k_{22} \cdot OH}{k_{20} \cdot M \cdot O_2} O_3 \quad (5)$$

235 By substituting this equation and Eq. (4) into Eq. (1) we obtain an expression relating OH, HO₂, and
236 O₃:

237
$$F(OH, HO_2, O_3) = \left(\frac{k_{20} \cdot M \cdot O_2}{k_{20} \cdot M \cdot O_2 + k_{21} \cdot O_3 + 2 \cdot k_{14} \cdot HO_2} + \frac{k_{12} \cdot M \cdot O_2 \cdot k_{22}}{(k_{52} + k_{53}) \cdot k_{17}} \right) \cdot \frac{k_{17} \cdot OH}{k_{18} \cdot HO_2} = 1 \quad (6)$$

238 Figure 1 shows height–latitude cross-sections of $\langle F(OH, HO_2, O_3) \rangle$ for each month (in this
239 Section angle brackets denote monthly averaged zonal mean values). The gray area corresponds
240 to $\chi > 85^\circ$. One can see that eq. (15) is most accurate within the 50–76 km range and above

241 86 km, where $|\langle F \rangle - 1| \leq 1\%$. The difference reaches 3–4 % in the region between 76 km and
 242 86 km. The altitude of this region has an annual variation with a maximum deviation in the winter
 243 hemisphere. Below 50 km the value of $\langle F \rangle$ increases up to 1.2 at 40 km, thus below the
 244 stratopause Eq. (6) no longer describes the simultaneous photochemical equilibrium of OH, HO₂
 245 and O₃. Note that these components remain short-lived below 50 km (with the lifetimes of about
 246 10^2 – 10^3 s (Brasseur and Solomon, 2005)) depending on height and duration of daylight. However,
 247 for quantitative description of their daytime equilibrium it is necessary to include additional
 248 reactions involving, in particular, the components of the NO_x family.

249 Note also that Eq. (1) and Eq. (6) take into account only the main daytime source of OH
 250 (P_{OH}) specified by reactions R18, R14, and R21:

$$251 P_{OH} = k_{18} \cdot HO_2 \cdot O + 2k_{14} \cdot HO_2 \cdot H + k_{21} \cdot O_3 \cdot H$$

252 These reactions run “inside” the HO_x (H, OH, HO₂, H₂O₂) family and do not perturb its total
 253 concentration. The height–latitude cross-sections of $\langle P_{OH} \rangle$ for each month are presented in
 254 Fig. 2.

255 The next important daytime source of OH is specified by reactions R59 and R7 involving H₂O, the
 256 main source for the HO_x family:

$$257 P_{OH}^{H_2O} = (k_{59} + 2 \cdot k_7 \cdot O(^1D)) \cdot H_2O$$

258 Figure 3 shows height–latitude cross-sections of $\langle P_{OH}^{H_2O} / P_{OH} \rangle$ for each month. Comparing Fig. 1
 259 and Fig. 3, we conclude that the previously indicated 3–4 % deviation of $\langle F \rangle$ from 1 in the region
 260 between 76 km and 86 km is largely due to the neglect of these reactions.

261 Another source of OH is sporadically activated during charged particle precipitation events
 262 and exists for a relatively short time (several days). Solar proton events (SPE) perturb the ionic
 263 composition in the mesosphere and the upper stratosphere considerably and trigger a whole
 264 cascade of reactions involving ions, neutral components and their clusters (e.g., O₂⁺·H₂O). This
 265 leads to an additional (to reactions R59 and R7) conversion of H₂O molecules into OH and H
 266 (Solomon et al., 1981). The maximum of the OH production rate (P_{OH}^{SPE}) induced by SPE is
 267 located in the polar latitudes in the region of 60–80 km and, as a rule, does not exceed $2 \cdot 10^3$ cm⁻³
 268 s⁻¹ (Jackman et al., 2011, 2014). It can be seen from Fig. 2 that at these latitudes and altitudes the
 269 P_{OH}^{SPE} / P_{OH} ratio does not exceed 1–2%, even for the maximum values of P_{OH}^{SPE} . This means that

270 the impact of P_{OH}^{SPE} on Eq. (6) is of the same order of smallness as in the case of reactions R59
 271 and R7, hence, it may be neglected. A similar conclusion can be made for other reactions from
 272 Table 1, not accounted for by Eq. (6), including the ones involving NO_x in both quiet and perturbed
 273 conditions in the mesosphere.

274

275 **4. Method of statistical evaluation of simultaneous measurement of OH, HO₂ and O₃**

276

277 The proposed method is based on the statistical Bayesian procedure described in the works by
 278 Kulikov et al. (2009) and Nechaev et al. (2016). It was originally developed for retrieving trace gas
 279 concentrations in the mesosphere from ground-based and satellite measurements of other
 280 mesospheric components. With respect to the considered evaluation problem this procedure
 281 consists of three steps: (1) constructing conditional probability density function (PDF) of OH, HO₂
 282 and O₃ concentration values at each altitude z in the selected interval assuming that there is
 283 certain measurement data of these components and the algebraic relationship (6) is valid; (2)
 284 calculating the first moments of this distribution, i.e. expected value and dispersion of each
 285 component using the Metropolis-Hastings algorithm (Chib and Greenberg, 1995) for
 286 multidimensional integration; (3) comparing the obtained results with the initial measurement data.

287 For constructing posterior PDF it is convenient to introduce vector $\vec{u}\{HO_2^{ret}, O_3^{ret}, OH^{ret}\}$,
 288 whose components are the retrieved values of chemical species concentrations at a certain altitude
 289 z , and vector $\vec{x}\{HO_2^m, O_3^m, OH^m\}$ composed of experimentally measured values of the components
 290 of vector \vec{u} , $x_j = u_j + \xi_j$, $j=1,3$, where ξ_j is a random error of measuring the j -th component of
 291 vector \vec{u} at the altitude z . It is assumed that

292 (1) random variables ξ_j are distributed normally with densities

$$293 \quad w_j(\xi_j) = \frac{1}{\sigma_j \sqrt{2\pi}} \exp\left(-\frac{\xi_j^2}{2\sigma_j^2}\right); \quad (7)$$

294 (2) ξ_j are mutually independent:

$$295 \quad \vec{\xi}\{\xi_1, \xi_2, \xi_3\} \sim W_{\xi}(\vec{\xi}) = \prod_j w_j(\xi_j), \quad (8)$$

296 where $W_{\xi}(\vec{\xi})$ is the total PDF of all ξ_j ;

297 (3) dispersions σ_j in Eq. (7), that are expected error values, are assumed to be known a priori (in
 298 our case they are provided by the MLS retrieval algorithm along with measured data).

299 Then the probability to observe vector \bar{x} is given by the conditional PDF

$$300 P_x(\bar{x} | \bar{u}) = \int \delta(\bar{x} - \bar{u}) W_\xi(\bar{\xi}') d^3 \bar{\xi}' = W_\xi(\bar{x} - \bar{u}), \quad (9)$$

301 where $\delta(\dots)$ is delta function.

302 The prior relationship of HO_2^{ret} , O_3^{ret} and OH^{ret} concentrations (Eq. (6)) can be written as

303 $u_3 = G(u_1, u_2)$. Integrating the left-hand side of Eq. (17) with conditional PDF of the variable u_3 :

$$304 P_{u_3}(u_3 | u_1, u_2) = \delta(u_3 - G(u_1, u_2)),$$

305 yields a likelihood function of the model

$$306 P_x(\bar{x} | u_1, u_2) = w_3(x_3 - G(u_1, u_2)) \cdot w_1(x_1 - u_1) w_2(x_2 - u_2). \quad (10)$$

307 According to Bayes' theorem, the posterior function, i.e. the probability density of latent variables u_1

308 and u_2 , under the condition that \bar{x} is observed, is defined by the expression

$$309 P(u_1, u_2 | \bar{x}) \propto P_x(\bar{x} | u_1, u_2) \cdot P_{apr}(u_1, u_2) \\ \propto \exp\left(-\frac{(x_1 - u_1)^2}{2\sigma_1^2}\right) \cdot \exp\left(-\frac{(x_2 - u_2)^2}{2\sigma_2^2}\right) \cdot \exp\left(-\frac{(x_3 - G(u_1, u_2))^2}{2\sigma_3^2}\right) \cdot P_{apr}(u_1, u_2) \quad (11)$$

310 in which $P_{apr}(u_1, u_2)$ defines prior PDF of u_1 and u_2 .

311 The retrieved value of the latent variable $u_{1,2,3}$ is hereinafter understood as the mean value

312 of the function in Eq. (11):

$$313 \langle u_{1,2} \rangle = \int_{-\infty}^{\infty} \int_{-\infty}^{\infty} u_{1,2} \cdot P(u_1, u_2 | \bar{x}) du_1 du_2 \\ \langle u_3 \rangle = \int_{-\infty}^{\infty} \int_{-\infty}^{\infty} G(u_1, u_2) \cdot P(u_1, u_2 | \bar{x}) du_1 du_2. \quad (12)$$

314 Its dispersion defines the uncertainty of the retrieval:

$$315 \sigma_{u_j} = \sqrt{\langle u_j^2 \rangle - \langle u_j \rangle^2}, \quad j = 1, 3, \quad (13)$$

316 where the angle brackets denote averaging in the sense of Eq. (12).

317

318 5. MLS/Aura data evaluation and results

320 We used the latest version (v4.2) of the MLS “standard” product (Livesey et al., 2017) for trace gas
 321 concentrations and temperature T within the 1 – 0.046 mbar pressure interval where all data are
 322 suitable for scientific applications (Wang et al., 2015a,b; Schwartz et al., 2015). We took the
 323 daytime data when the solar zenith angle $\chi < 80^\circ$ for January, May, and September 2005. All data
 324 were appropriately screened. “Pressure”, “estimated precision”, “status flag”, “quality”,
 325 “convergence” and “clouds” fields were taken into account. HO₂ data were seen as the day-minus-
 326 night difference as prescribed by the MLS data guidelines (Livesey et al., 2017). Following Pickett
 327 et al. (2008), each daytime profile of this component measured on a given day at a latitude Lat, a
 328 profile resulting from averaging the nighttime profiles of HO₂, measured on the same day in the
 329 latitude range of Lat \pm 5°, was subtracted. This operation eliminates systematic biases affecting HO₂
 330 retrievals, but limits the studied latitude range to the one where MLS observes both daytime and
 331 nighttime data.

332 The integrals in Eq. (12)–(13) were calculated at every pressure level p for each set of
 333 simultaneously measured vertical profiles $OH^{MLS}(p)$, $HO_2^{MLS}(p)$, $O_3^{MLS}(p)$, $T^{MLS}(p)$, $\sigma_{OH^{MLS}}(p)$,
 334 $\sigma_{HO_2^{MLS}}(p)$, $\sigma_{O_3^{MLS}}(p)$. The vertical profiles $\langle OH^{ret} \rangle(p)$, $\langle HO_2^{ret} \rangle(p)$, $\langle O_3^{ret} \rangle(p)$, $\sigma_{OH^{ret}}(p)$,
 335 $\sigma_{HO_2^{ret}}(p)$, $\sigma_{O_3^{ret}}(p)$ were found at each point of the globe along the satellite track. Numerical
 336 integration was performed by a Monte Carlo method. For each pressure level, a sample of about
 337 $5 \cdot 10^5$ pairs of random variable values $\{u_1, u_2\} = \{HO_2^{ret}, O_3^{ret}\}$ distributed with normalized probability
 338 density given by Eq. (11) with $P_{apr}(u_1, u_2) \equiv 1$ was generated with the help of the Metropolis-
 339 Hastings algorithm (Chib and Greenberg, 1995). In this case, the statistical moments in Eq. (12)–
 340 (13) were determined by summation over the sample.

341 A typical example of retrieved profiles HO_2^{ret} , O_3^{ret} and OH^{ret} (black curves) in comparison
 342 with the measured HO_2^{MLS} , O_3^{MLS} and OH^{MLS} (red curves) is given in Fig. 4. First of all, note that
 343 statistics of the retrieved data is in satisfactory agreement with the initial measurement of OH and
 344 O₃ concentrations, but not of HO₂. The error of satellite measurement, $\sigma_{HO_2^{MLS}}$, greatly exceeds the
 345 uncertainty of retrieval, $\sigma_{HO_2^{ret}}$, so at some altitudes the values of $\langle HO_2^{MLS} \rangle$ (red dashed curves)
 346 do not fall within the corresponding intervals $\langle HO_2^{ret} \rangle \pm \sigma_{HO_2^{ret}}$. Second, the results of a single

347 measurement of all three components and their retrieved values have considerable uncertainties
 348 relative to their means within the whole interval of altitudes. Therefore, the observed and retrieved
 349 data should be compared using the commonly accepted approach (e.g., Pickett et al., 2008) of
 350 averaging large ensembles of profiles within certain latitude and time ranges, or zones. It is
 351 supposed that the noise of satellite measurement instruments is delta-correlated, so that random
 352 values corresponding to each single measured or retrieved profile are statistically independent. In
 353 this case the dispersion of a measured or retrieved zonal mean profile is determined by summation

$$354 \quad \sigma_{\Sigma}^2 = \frac{1}{N^2} \sum_{k=1}^N \sigma_k^2,$$

355 where N is the number of measured or retrieved profiles within the zone and σ_k^2 is the dispersion
 356 of the k -th measured or retrieved profile.

357 The range of latitudes covered by the satellite trajectory was divided into 17 bins 10° each.
 358 About 3000 single profiles of each chemical component fall into one bin during a month of
 359 MLS/Aura observations. Therefore, the resulting uncertainties due to measurement noise of OH,
 360 HO₂ and O₃ concentration profiles (both measured and retrieved) averaged over such ensembles
 361 are significantly (about one and a half order of magnitude) lower than the uncertainties of individual
 362 profiles. Examples of such profiles for January, May and September 2005 are presented in Fig. 5.
 363 One can see that the indicated uncertainties are now small enough to make clear conclusions
 364 about the extent to which the observed and retrieved profiles agree by comparing their averaged
 365 values only, i.e. $\langle OH^{MLS} \rangle$, $\langle HO_2^{MLS} \rangle$, $\langle O_3^{MLS} \rangle$ and $\langle OH^{ret} \rangle$, $\langle HO_2^{ret} \rangle$, $\langle O_3^{ret} \rangle$.

366 Figures 4–6 show monthly averaged zonal mean pressure–latitude cross-sections of
 367 $\langle HO_2^{ret} \rangle$, $\langle HO_2^{MLS} \rangle$, $\Delta HO_2 = (\langle HO_2^{ret} \rangle - \langle HO_2^{MLS} \rangle) / \langle HO_2^{MLS} \rangle$ and similar characteristics
 368 for OH and O₃ concentration profiles for three months of the year 2005. First, clearly, the
 369 distributions of $\langle OH^{ret} \rangle$ and $\langle O_3^{ret} \rangle$ are in good qualitative and quantitative agreement with the
 370 initial MLS/Aura measurement data at lower altitudes, below ~ 0.07 mbar and 0.1 mbar,
 371 correspondingly. At higher altitudes, the distributions of $\langle OH^{ret} \rangle$ reproduce all the main structural
 372 features of $\langle OH^{MLS} \rangle$, but the retrieved OH concentration has lower values than the observed one
 373 with a relative difference ΔOH reaching $\sim 15\%$ at the top. The distribution of $\langle O_3^{ret} \rangle$ above
 374 0.1 mbar, in turn, differs considerably from $\langle O_3^{MLS} \rangle$, both in quantity and quality, and ΔO_3 locally

375 reaches 50-60% and more. Second, for all months there are significant qualitative and quantitative
376 differences between $\langle HO_2^{ret} \rangle$ and $\langle HO_2^{MLS} \rangle$, the most noticeable one being location of the
377 mesospheric maximum of this component's concentration. According to the observations it is close
378 to 0.1 mbar, while the retrieved data demonstrate the altitudes of about ~0.046 mbar or higher. Our
379 analysis of the applied method of statistical evaluation demonstrates that the higher position of this
380 maximum in the distributions of $\langle HO_2^{ret} \rangle$ is influenced by the OH^{MLS} data in which the
381 mesospheric maximum (see Figs. 6-8) is also located notably higher than 0.1 mbar.

382

383 6. Discussion and conclusion

384

385 On the basis of the data presented in Section 5 we can conclude that, upon the whole,
386 simultaneous OH, HO₂ and O₃ satellite measurements poorly satisfy the photochemical equilibrium
387 condition. The HO₂ component biases from this condition most prominently. We can conjecture that
388 a possible explanation for the bias is the significant systematic error in HO₂ measurements, in
389 particular, in the height of the mesospheric maximum. This assumption is supported by the
390 calculation of the HO₂ distributions with the use of our 3D chemical transport model (see Fig. 9). It
391 can be seen that the mesospheric maximum of HO₂ in these months, as well as of the $\langle HO_2^{ret} \rangle$
392 distributions, lies above 0.046 mbar.

393 Moreover, new data on the HO₂ distributions were recently obtained from the MLS
394 measurements. Millán et al. (2015) performed the offline retrieval of daily zonal means of HO₂
395 profiles using averaged MLS radiances measured in 10° latitude bins. Averaged spectra have a
396 better signal to noise ratio, which removes many of the limitations of the MLS standard product for
397 HO₂. In particular, the upper boundary of the altitude region in which daytime data is suitable for
398 scientific use has reached 0.0032 mbar, and the "day-minus-night" correction is not needed at
399 altitudes above 1 mbar. Comparison with various experimental and model data has shown that the
400 offline retrieval reproduces the basic properties of the HO₂ distribution in the mesosphere relatively
401 well (at least qualitatively) (Millán et al. 2015).

402 The offline retrieval product, the alternative dataset of daytime HO₂, has recently become
403 publicly available at <https://mls.jpl.nasa.gov>. Figure 10 shows the monthly averaged zonal means
404 of offline retrieval data ($\langle HO_2^{MLS}_{offline} \rangle$) and relative differences with retrieved and MLS standard

405 product data $(\langle HO_2^{MLS} \rangle - \langle HO_2^{MLS}_{offline} \rangle) / \langle HO_2^{MLS}_{offline} \rangle$ and
 406 $(\langle HO_2^{ret} \rangle - \langle HO_2^{MLS}_{offline} \rangle) / \langle HO_2^{MLS}_{offline} \rangle$, correspondingly. Figure 10 represents the same time
 407 periods as Figs. 6-8. It is worth noting that the distributions $\langle HO_2^{MLS}_{offline} \rangle$ depicted in Fig. 10
 408 represent significantly different amounts of data. The data sets for May and September include 31
 409 and 27 days of measurements, respectively, whereas the January dataset encompasses only 4
 410 days. The latter makes the graphs in the first row in Fig. 10 noisier than the others. One can see
 411 that the results of the offline HO₂ retrieval show the same features as the results of our evaluation
 412 technique in comparison to the standard MLS retrieval, i.e. the height of mesospheric HO₂
 413 maximum is notably higher. We can conclude that the distributions of $\langle HO_2^{ret} \rangle$ better match
 414 $\langle HO_2^{MLS}_{offline} \rangle$ than $\langle HO_2^{MLS} \rangle$, although some quantitative discrepancy between $\langle HO_2^{ret} \rangle$ and
 415 $\langle HO_2^{MLS}_{offline} \rangle$ also exists. Note that this may be due to systematic errors in the HO_2^{MLS}
 416 distributions, which cannot be excluded within the framework of the introduced technique. For a
 417 detailed qualitative and quantitative comparison of $\langle HO_2^{ret} \rangle$ and $\langle HO_2^{MLS}_{offline} \rangle$ one should
 418 modify the method, so that a statistical evaluation of the OH^{MLS} and O_3^{MLS} standard products, and
 419 the data of the offline HO₂ retrieval could be conducted within the framework of a single procedure
 420 with no account for the HO_2^{MLS} distributions. This modification is under way and will be presented
 421 elsewhere.

422 The proposed method for statistical evaluation of mesospheric species measurements can
 423 be readily generalized to other atmospheric photochemical systems that contain short-lived
 424 components (see Introduction). It may also be modified for assessing hard to measure chemical
 425 components, characteristics of atmospheric processes (like wind speed or turbulent diffusion rate),
 426 or poorly known reaction rates.

427

428 Acknowledgments

429 The work was carried out within the framework of the state assignment of IAP RAS (project 0035-
 430 2014-0033) and was supported partially by the Russian Foundation for Basic Research (project
 431 №17-05-01142). The data used in this study is supported by the Institute of Applied Physics of the
 432 Russian Academy of Sciences (Nizhny Novgorod, Russia). Inquiries about the distributions used in
 433 this paper can be addressed to Mr. Belikovich (belikovich@ipfran.ru).

434

435 **References**

436

437 Avallone, L. M., and Toohey, D. W.: Tests of halogen photochemistry using in situ
438 measurements of ClO and BrO in the lower polar stratosphere, *J. Geophys. Res.*, Volume 106,
439 Issue D10, Pages 10411–1042, doi: 10.1029/2000JD900831, 2001.

440 Benton, A. K., Langridge, J. M., Ball, S. M., Bloss, W. J., Dall'Osto, M., Nemitz, E., Harrison,
441 R. M., and Jones, R. L.: Night-time chemistry above London: measurements of NO₃ and N₂O₅
442 from the BT Tower, *Atmos. Chem. Phys.*, 10, 9781-9795, doi:10.5194/acp-10-9781-2010, 2010.

443 Berger, U.: Numerische Simulation klimatologischer Prozesse und thermische Gezeiten in
444 der mittleren Atmosphäre, Thesis, Univ. Cologne, Germany, 1994.

445 Berger, U. and von Zahn, U.: The two-level structure of the mesopause: A model study, *J.*
446 *Geophys. Res.*, 104, 22083–22093, 1999.

447 Berthet, G., Ricaud, P., Lefevre, F., Le Flochmoen, E., Urban, J., Barret, B., Lautie, N.,
448 Dupuy, E., De La Noe, J., and Murtagh, D.: Nighttime chlorine monoxide observations by the Odin
449 satellite and implications for the ClO/Cl₂O₂ equilibrium, *Geophys. Res. Lett.*, 32, L11812,
450 doi:10.1029/2005GL022649, 2005.

451 Brasseur, G. and Solomon, S.: *Aeronomy of the Middle Atmosphere*, 644 pp., 3rd edition,
452 Springer, The Netherlands, 2005.

453 Brown, S. S., Stark, H., Ryerson, T. B., Williams, E. J., Nicks Jr., D. K., Trainer, M.,
454 Fehsenfeld, F. C., and Ravishankara, A. R.: Nitrogen oxides in the nocturnal boundary layer:
455 Simultaneous in situ measurements of NO₃, N₂O₅, NO₂, NO, and O₃, *J. Geophys. Res.*, 108(D9),
456 4299, doi:10.1029/2002JD002917, 2003.

457 Burkholder, J. B., S. P. Sander, J. Abbatt, J. R. Barker, R. E. Huie, C. E. Kolb, M. J. Kurylo,
458 V. L. Orkin, D. M. Wilmouth, and P. H. Wine, *Chemical Kinetics and Photochemical Data for Use in*
459 *Atmospheric Studies*, Evaluation No. 18, JPL Publication 15-10, Jet Propulsion Laboratory,
460 Pasadena, <http://jpldataeval.jpl.nasa.gov>, 2015.

461 Butz, A., H. Bosch, C. Camy-Peyret, M. Dorf, A. Engel, S. Payan, and Pfeilsticker, K.:
462 Observational constraints on the kinetics of the ClO-BrO and ClO-ClO ozone loss cycles in the
463 Arcticwinter stratosphere, *Geophys. Res. Lett.*, 34, L05801, doi:10.1029/2006GL028718, 2007.

464 Cantrell, C. A., Mauldin, L., Zondlo, M., Eisele, F., Kosciuch, E., Shetter, R., Lefer, B., Hall,
465 S., Campos, T., Ridley, B., Walega, J., Fried, A., Wert, B., Flocke, F., Weinheimer, A., Hannigan,
466 J., Coffey, M., Atlas, E., Stephens, S., Heikes, B., Snow, J., Blake, D., Blake, N., Katzenstein, A.,
467 Lopez, J., Browell, E. V., Dibb, J., Scheuer, E., Seid, G., and Talbot, R.: Steady state free radical
468 budgets and ozone photochemistry during TOPSE, *J. Geophys. Res.*, 108(D4), 8361,
469 doi:10.1029/2002JD002198, 2003.

470 Chameides, W.: Tropospheric odd nitrogen and the atmospheric water vapor cycle, *J.*
471 *Geophys. Res.*, 84 (C10), 4989–4996, doi: 10.1029/JC080i036p04989, 1975.

472 Chib, S., and Greenberg, E.: Understanding the Metropolis-Hastings Algorithm, *The*
473 *American Statistician*, 49 (4), 327-335, doi: 10.2307/2684568, 1995.

474 Crawford, J., Davis, D., Chen, G., Bradshaw, J., Sandholm, S., Gregory, G., Sachse, G.,
475 Anderson, B., Collins, J., Blake, D., Singh, H., Heikes, B., Talbot, R., Rodriguez, J.: Photostationary
476 state analysis of the NO₂-NO system based on airborne observations from the western and central
477 North Pacific, 101(D1), 2053–2072, doi: 10.1029/95JD02201, 1996.

478 Crowley, J. N., Schuster, G., Pouvesle, N., Parchatka, U., Fischer, H., Bonn, B., Bingemer,
479 H., and Lelieveld, J.: Nocturnal nitrogen oxides at a rural mountain-site in south-western Germany,
480 *Atmos. Chem. Phys.*, 10, 2795-2812, doi:10.5194/acp-10-2795-2010, 2010.

481 de Grandpre, J., Beagley, S. R., Fomichev, V. I., Griffioen, E., McConnell, J. C., Medvedev,
482 A. S., and Shepherd, T. G.: Ozone climatology using interactive chemistry: Results from the
483 Canadian Middle Atmosphere Model, *J. Geophys. Res.-Atmos.*, 105, 26475-26491,
484 doi:10.1029/2000JD900427, 2000.

485 Djouad, R., Michelangeli, D. V., and Gong, W.: Numerical solution for atmospheric
486 multiphase models: Testing the validity of equilibrium assumptions, *J. Geophys. Res.*, 108(D19),
487 4602, doi:10.1029/2002JD002969, 2003.

488 Douglass, A. R., Jackman, C. H., and Stolarski, R. S.: Comparison of model results
489 transporting the odd nitrogen family with results transporting separate odd nitrogen species, *J.*
490 *Geophys. Res.*, 94(D7), 9862–9872, doi:10.1029/JD094iD07p09862, 1989.

491 Ebel, A., Berger, U., and Krueger, B. C.: Numerical simulations with COMMA, a global
492 model of the middle atmosphere, *SIMPO Newsletter*, 12, 22–32, 1995.

493 Evans, W. F. J., and Llewellyn, E. J.: Atomic hydrogen concentrations in the mesosphere
494 and the hydroxyl emissions, *J. Geophys. Res.*, 78, 323–326, doi:10.1029/JA078i001p00323, 1973.

495 Evans, W. F. J., McDade, I. C., Yuen, J., and Llewellyn, E. J.: A rocket measurement of the
496 O₂ infrared atmospheric (0-0) band emission in the dayglow and a determination of the
497 mesospheric ozone and atomic oxygen densities, *Can. J. Phys.*, 66, 941–946, doi:10.1139/p88-15,
498 1988.

499 Feigin, A. M., and Konovalov, I. B.: On the possibility of complicated dynamic behavior of
500 atmospheric photochemical systems: Instability of the Antarctic photochemistry during the ozone
501 hole formation, *J. Geophys. Res.*, 101, 26023–26038, doi:10.1029/96JD02011, 1996.

502 Feigin, A. M., Konovalov, I. B., and Molkov, Ya. I.: Towards understanding nonlinear nature
503 of atmospheric photochemistry: Essential dynamic model of the mesospheric photochemical
504 system, *J. Geophys. Res.*, 103, 25447–25460, doi:10.1029/98JD01569, 1998.

505 Funke, B., Lopez-Puertas, M., von Clarmann, T., Stiller, G. P., Fischer, H., Glatthor, N.,
506 Grabowski, U., Hopfner, M., Kellmann, S., Kiefer, M., Linden, A., Mengistu Tsidu, G., Milz, M.,
507 Steck, T. and Wang, D. Y.: Retrieval of stratospheric NO_x from 5.3 and 6.2 mm nonlocal
508 thermodynamic equilibrium emissions measured by Michelson Interferometer for Passive
509 Atmospheric Sounding (MIPAS) on Envisat, *J. Geophys. Res.*, 110, D09302,
510 doi:10.1029/2004JD005225, 2005.

511 Ghosh, S., Pyle, J. A., and Good, P.: Temperature dependence of the ClO concentration
512 near the stratopause, *J. Geophys. Res.*, 102(D15), 19207–19216, doi:10.1029/97JD01099, 1997.

513 Good, R. E.: Determination of atomic oxygen density from rocket borne measurements of
514 hydroxyl airglow, *Planet. Space Sci.*, 24, 389–395, doi.org/10.1016/0032-0633(76)90052-0, 1976.

515 Grygalashvyly, M., Sonnemann, G. R., and Hartogh, P.: Long-term behavior of the
516 concentration of the minor constituents in the mesosphere—A model study, *Atmos. Chem. Phys.*,
517 9, 2779–2792, doi:10.5194/acp-9-2779-2009, 2009.

518 Grygalashvyly, M., Becker, E., and Sonnemann, G. R.: Wave mixing effects on minor
519 chemical constituents in the MLT region: Results from a global CTM driven by high-resolution
520 dynamics, *J. Geophys. Res.*, 116, D18302, doi:10.1029/2010JD015518, 2011.

521 Grygalashvyly, M., Becker, E., and Sonnemann, G. R.: Gravity wave mixing and effective
522 diffusivity for minor chemical constituents in the mesosphere/lower thermosphere, *Space Sci. Rev.*,
523 168, 333–362, doi:10.1007/s11214-011-9857-x, 2012.

524 Grygalashvyly, M., Sonnemann, G. R., Lübken, F.-J., Hartogh, P., and Berger, U.: Hydroxyl
525 layer: Mean state and trends at midlatitudes, *J. Geophys. Res.-Atmos.*, 119, 12391–12419,
526 doi:10.1002/2014JD022094, 2014.

527 Grygalashvyly, M.: Several notes on the OH* layer, *Ann. Geophys.*, 33, 923-930,
528 doi:10.5194/angeo-33-923-2015, 2015.

529 Hartogh, P., Jarchow, C., Sonnemann, G. R., and Grygalashvyly, M.: On the spatiotemporal
530 behavior of ozone within the upper mesosphere/mesopause region under nearly polar night
531 conditions, *J. Geophys. Res.*, 109, D18303, doi:10.1029/2004JD004576, 2004.

532 Hartogh, P., Sonnemann, G. R., Grygalashvyly, M., and Jarchow, Ch.: Ozone trends in mid-
533 latitude stratopause region based on microwave measurements at Lindau (51.66° N, 10.13° E), the
534 ozone reference model, and model calculations, *Adv. Space Res.*, 47, 1937-1948,
535 doi:10.1016/j.asr.2011.01.010, 2011.

536 Hauchecorne, A., Bertaux, J. L., Dalaudier, F., Keckhut, P., Lemennais, P., Bekki, S.,
537 Marchand, M., Lebrun, J. C., Kyrölä, E., Tamminen, J., Sofieva, V., Fussen, D., Vanhellefont, F.,
538 Fanton d'Andon, O., Barrot, G., Blanot, L., Fehr, T., and Saavedra de Miguel, L.: Response of
539 tropical stratospheric O₃, NO₂ and NO₃ to the equatorial Quasi-Biennial Oscillation and to
540 temperature as seen from GOMOS/ENVISAT, *Atmos. Chem. Phys.*, 10, 8873-8879,
541 doi:10.5194/acp-10-8873-2010, 2010.

542 Jackman, C. H., Marsh, D. R., Vitt, F. M., Roble, R. G., Randall, C. E., Bernath, P. F., Funke,
543 B., López-Puertas, M., Versick, S., Stiller, G. P., Tylka, A. J., and Fleming, E. L.: Northern
544 Hemisphere atmospheric influence of the solar proton events and ground level enhancement in
545 January 2005, *Atmos. Chem. Phys.*, 11, 6153-6166, <https://doi.org/10.5194/acp-11-6153-2011>,
546 2011.

547 Jackman, C. H., Randall, C. E., Harvey, V. L., Wang, S., Fleming, E. L., López-Puertas, M.,
548 Funke, B., and Bernath, P. F.: Middle atmospheric changes caused by the January and March
549 2012 solar proton events, *Atmos. Chem. Phys.*, 14, 1025-1038, [https://doi.org/10.5194/acp-14-](https://doi.org/10.5194/acp-14-1025-2014)
550 [1025-2014](https://doi.org/10.5194/acp-14-1025-2014), 2014.

551 Kawa, S. R., Fahey, D. W., Solomon, S., Brune, W. H., Proffitt, M. H., Toohey, D. W.,
552 Anderson Jr., D. E., Anderson, L. C., and Chan, K. R.: Interpretation of aircraft measurements of
553 NO, ClO, and O₃ in the lower stratosphere, *J. Geophys. Res.*, 95(D11), 18597–18609 doi:
554 10.1029/JD095iD11p18597, 1990.

555 Kremp, C., Berger, U., Hoffmann, P., Keuer, D., and Sonnemann, G. R.: Seasonal variation
556 of middle latitude wind fields of the mesopause region – a comparison between observation and
557 model calculation, *Geophys. Res. Lett.*, 26, 1279–1282, 1999.

558 Kaye, J. A., and Rood, R. B.: Chemistry and transport in a three-dimensional stratospheric
559 model: Chlorine species during a simulated stratospheric warming, *J. Geophys. Res.*, 94(D1),
560 1057–1083, doi: 10.1029/JD094iD01p01057, 1989.

561 Ko, M., Hu, W., Rodriguez, J. M., Kondo, Y., Koike, M., Kita, K., Kawakami, S., Blake, D.,
562 Liu, S., and Ogawa, T.: Photochemical ozone budget during the BIBLE A and B campaigns, *J.*
563 *Geophys. Res.*, 107, 8404, doi:10.1029/2001JD000800, 2002. [printed 108(D3), 2003].

564 Kondo, Y., Matthews, W. A., Amedieu, P., and Robbins, D. E. Diurnal variation of nitric
565 oxide at 32 km: Measurements and interpretation, *J. Geophys. Res.*, 93(D3), 2451–2460,
566 doi:10.1029/JD093iD03p02451, 1988.

567 Kondo, Y., Ziereis, H., Koike, M., Kawakami, S., Gregory, G. L., Sachse, G. W., Singh, H.
568 B., Davis, D. D., Merrill, J. T.: Reactive nitrogen over the Pacific Ocean during PEM-West, A
569 101(D1), 1809–1828, doi:10.1029/95JD02611, 1996.

570 Konovalov, I. B., Feigin, A. M., Mukhina, A. Y.: Toward understanding of the nonlinear
571 nature of atmospheric photochemistry: Multiple equilibrium states in the high-latitude lower
572 stratospheric photochemical system, *J. Geophys. Res.*, 104, 8669-8689,
573 doi:10.1029/1998JD100037, 1999.

574 Konovalov, I. B., and Feigin, A. M.: Toward an understanding of the nonlinear nature of
575 atmospheric photochemistry: Origin of the complicated dynamic behaviour of the mesospheric
576 photochemical system, *Nonlin. Processes Geophys.*, 7, 87–104, doi:10.5194/npg-7-87-2000, 2000.

577 Körner, U., and Sonnemann, G. R.: Global 3D-modeling of water vapor concentration of the
578 mesosphere/mesopause region and implications with respect to the NLC region, *J. Geophys. Res.-*
579 *Atmos.*, 106, 9639– 9651, doi:10.1029/2000JD900744, 2001.

580 Kowalewski, S., von Savigny, C., Palm, M., McDade, I. C., and Notholt, J.: On the impact of
581 the temporal variability of the collisional quenching process on the mesospheric OH emission layer:
582 a study based on SD-WACCM4 and SABER, *Atmos. Chem. Phys.*, 14, 10193-10210,
583 doi:10.5194/acp-14-10193-2014, 2014.

584 Kremser, S., Schofield, R., Bodeker, G. E., Connor, B. J., Rex, M., Barret, J., Mooney, T.,
585 Salawitch, R. J., Canty, T., Frieler, K., Chipperfield, M. P., Langematz, U., and Feng, W.: Retrievals

586 of chlorine chemistry kinetic parameters from Antarctic ClO microwave radiometer measurements,
587 *Atmos. Chem. Phys.*, 11, 5183-5193, doi:10.5194/acp-11-5183-2011, 2011.

588 Kulikov, M. Y., Feigin, A. M., and Sonnemann, G. R.: Retrieval of the vertical distribution of
589 chemical components in the mesosphere from simultaneous measurements of ozone and hydroxyl
590 distributions, *Radiophys. Quantum Electron.*, 49, 683–691, doi:10.1007/s11141-006-0103-4, 2006.

591 Kulikov, M. Yu., Feigin, A. M., and Sonnemann, G. R.: Retrieval of water vapor profile in the
592 mesosphere from satellite ozone and hydroxyl measurements by the basic dynamic model of
593 mesospheric photochemical system, *Atmos. Chem. Phys.*, 9, 8199-8210, doi:10.5194/acp-9-8199-
594 2009, 2009.

595 Kulikov, M. Y., Mukhin, D. N., and Feigin, A. M.: Bayesian strategy of accuracy estimation
596 for characteristics retrieved from experimental data using base dynamic models of atmospheric
597 photochemical systems, *Radiophys. Quantum Electron.*, 52, 618–626, doi:10.1007/s11141-010-
598 9171-6, 2009.

599 Kulikov, M. Yu., Vadimova, O. L., Ignatov, S. K., and Feigin, A.M.: The mechanism of non-
600 linear photochemical oscillations in the mesopause region, *Nonlinear Processes in Geophysics*,
601 v.19, p.p.501–512, doi:10.5194/npg-19-501-2012, 2012.

602 Kulikov, M. Yu., and Feigin, A. M.: Automated construction of the basic dynamic models of
603 the atmospheric photochemical systems using the RADM2 chemical mechanism as an example,
604 *Radiophys. Quantum Electron.*, 57, 478-487, doi 10.1007/s11141-014-9530-9, 2014.

605 Kulikov, M. Y., Belikovich, M. V., Grygalashvyly, M., Sonnemann, G. R., Ermakova, T. S.,
606 Nechaev, A. A., and Feigin, A. M.: Daytime ozone loss term in the mesopause region, *Ann.*
607 *Geophys.*, 35, 677-682, doi:10.5194/angeo-35-677-2017, 2017.

608 Livesey, N. J., Read, W. G., Wagner, P. A., Frovideaux, L., Lambert, A., Manney, G. L.,
609 Millan, L. F., Pumphrey, H. C., Santee, M. L., Schwartz, M. J., Wang, S., Fuller, R. A., Jarnot, R. F.,
610 Knosp, B. W., and Martinez E.: Earth Observing System (EOS) Aura Microwave Limb Sounder
611 (MLS) Version 4.2 Level 2 data quality and description document, JPL D-33509, JPL publication,
612 USA, 2017.

613 Llewellyn, E. J., McDade, I. C., Moorhouse, P., and Lockerbie, M. D.: Possible reference
614 models for atomic oxygen in the terrestrial atmosphere, *Adv. Space Res.*, 13, 135–144,
615 doi:0.1016/0273-1177(93)90013-2, 1993.

616 Llewellyn, E. J., and McDade, I. C.: A reference model for atomic oxygen in the terrestrial
617 atmosphere, *Adv. Space Res.*, 18, 209–226, doi:10.1016/0273-1177(96)00059-2, 1996.

618 Lübken, F. J.: Seasonal variation of turbulent energy dissipation rates at high latitudes as
619 determined by in situ measurements of neutral density fluctuations, *J. Geophys. Res.*, 102, 13441–
620 13456, 1997.

621 Marchand, M., Bekki, S., Lefevre, F., and Hauchecorne, A.: Temperature retrieval from
622 stratospheric O₃ and NO₃ GOMOS data, *Geophys. Res. Lett.*, 34, L24809,
623 doi:10.1029/2007GL030280, 2007.

624 Marsh, D. R., Smith, A. K., Mlynczak, M. G., and Russell III, J. M.: SABER observations of
625 the OH Meinel airglow variability near the mesopause, *J. Geophys. Res.*, 111, A10S05,
626 doi:10.1029/2005JA011451, 2006.

627 Martinez, M., Perner, D., Hackenthal, E.-M., Kulzer, S., and Schultz, L.: NO₃ at Helgoland
628 during the NORDEX campaign in October 1996, *J. Geophys. Res.*, 105(D18), 22,685–22,695,
629 doi:10.1029/2000JD900255, 2000.

630 Massie, S. T., and Hunten, D. M.: Stratospheric eddy diffusion coefficients from tracer data,
631 *J. Geophys. Res.*, 86(C10), 9859–9868, doi:10.1029/JC086iC10p09859, 1981.

632 McDade, I. C., Llewellyn, E. J., and Harris, F. R.: Atomic oxygen concentrations in the lower
633 auroral thermosphere, *Adv. Space Res.*, 5(7), 229–232, doi:10.1016/0273-1177(85)90379-5, 1985.

634 McDade, I. C., and Llewellyn, E. J.: Mesospheric oxygen atom densities inferred from
635 night-time OH Meinel band emission rates, *Planet. Space Sci.*, 36, 897–905, DOI:10.1016/0032-
636 0633(88)90097-9, 1988.

637 McLaren, R., Wojtal, P., Majonis, D., McCourt, J., Halla, J. D., and Brook, J.: NO₃ radical
638 measurements in a polluted marine environment: links to ozone formation, *Atmos. Chem. Phys.*,
639 10, 4187-4206, doi:10.5194/acp-10-4187-2010, 2010.

640 Millán, L., Wang, S., Livesey, N., Kinnison, D., Sagawa, H., and Kasai, Y.: Stratospheric and
641 mesospheric HO₂ observations from the Aura Microwave Limb Sounder, *Atmos. Chem. Phys.*, 15,
642 2889-2902, doi:10.5194/acp-15-2889-2015, 2015.

643 Mlynczak, M. G., and Solomon, S.: Middle atmosphere heating by exothermic chemical
644 reactions involving odd-hydrogen species, *Geophys. Res. Lett.*, 18, 37-40,
645 doi:10.1029/90GL02672, 1991.

646 Mlynczak, M. G., and Solomon, S.: A detailed evaluation of the heating efficiency in the
647 middle atmosphere, *J. Geophys. Res.*, 98, 10,517–10,541, doi:10.1029/93JD00315, 1993.

648 Mlynczak, M. G., Marshall, B. T., Martin-Torres, F. J., Russell III, J. M., Thompson, R. E.,
649 Remsberg, E. E., and Gordley, L. L.: Sounding of the Atmosphere using Broadband Emission
650 Radiometry observations of daytime mesospheric O₂(1D) 1.27 μm emission and derivation of
651 ozone, atomic oxygen, and solar and chemical energy deposition rates, *J. Geophys. Res.*, 112,
652 D15306, doi:10.1029/2006JD008355, 2007.

653 Mlynczak, M. G., Hunt, L. A., Mast, J. C., Marshall, B. T., Russell III, J. M., Smith, A. K.,
654 Siskind, D. E., Yee, J.-H., Mertens, C. J., Martin-Torres, F. J., Thompson, R. E., Drob, D. P., and
655 Gordley, L. L.: Atomic oxygen in the mesosphere and lower thermosphere derived from SABER:
656 Algorithm theoretical basis and measurement uncertainty, *J. Geophys. Res.*, 118, 5724–5735,
657 doi:10.1002/jgrd.50401, 2013a.

658 Mlynczak, M. G., Hunt, L. H., Mertens, C. J., Marshall, B. T., Russell III, J. M., López-
659 Puertas, M., Smith, A. K., Siskind, D. E., Mast, J. C., Thompson, R. E., and Gordley, L. L.:
660 Radiative and energetic constraints on the global annual mean atomic oxygen concentration in the
661 mesopause region, *J. Geophys. Res. Atmos.*, 118, 5796–5802, doi:10.1002/jgrd.50400, 2013b.

662 Mlynczak, M. G., Hunt, L. A., Marshall, B. T., Mertens, C. J., Marsh, D. R., Smith, A. K.,
663 Russell, J. M., Siskind, D. E., and Gordley, L. L.: Atomic hydrogen in the mesopause region
664 derived from SABER: Algorithm theoretical basis, measurement uncertainty, and results, *J.*
665 *Geophys. Res.*, 119, 3516–3526, doi:10.1002/2013JD021263, 2014.

666 Morton, K. W., and D. F. Mayers, *Numerical Solution of Partial Differential Equations*,
667 Cambridge University Press, 1994.

668 Nechaev, A. A., Ermakova, T. S., and Kulikov, M. Y.: Determination of the Trace-Gas
669 Concentrations at the Altitudes of the Lower and Middle Mesosphere from the Time Series of
670 Ozone Concentration, *Radiophys. Quantum Electron.*, 59, 546–559, doi:10.1007/s11141-016-
671 9722-6, 2016.

672 Nikoukar, R., Swenson, G. R., Liu, A. Z., and Kamalabadi, F.: On the variability of
673 mesospheric OH emission profiles, *J. Geophys. Res.*, 112, D19109, doi:10.1029/2007JD008601,
674 2007.

675 Pendleton, W. R., Baker, K. D., and Howlett, L. C.: Rocket-based investigations of $O(^3P)$,
676 $O_2(a^1\Delta_g)$ and $OH^*(\nu=1,2)$ during the solar eclipse of 26 February 1979, *J. Atm. Terr. Phys.*, 45 (7),
677 479 – 491, doi:10.1016/S0021-9169(83)81108-8, 1983.

678 Penkett, S. A., Monks, P. S., Carpenter, L. J., Clemitshaw, K. C., Ayers, G. P., Gillett, R. W.,
679 Galbally, I. E., and Meyer, C. P.: Relationships between ozone photolysis rates and peroxy radical
680 concentrations in clean marine air over the Southern Ocean, *J. Geophys. Res.*, 102(D11), 12805–
681 12817, doi:10.1029/97JD00765, 1997.

682 Penkett, S. A., Reeves, C. E., Bandy, B. J., Kent, J. M., and Richer, H. R.: Comparison of
683 calculated and measured peroxide data collected in marine air to investigate prominent features of
684 the annual cycle of ozone in the troposphere, *J. Geophys. Res.*, 103(D11), 13377–13388,
685 doi:10.1029/97JD02852, 1998.

686 Platt, U., Perner, D., and Pätz, H. W.: Simultaneous measurement of atmospheric CH_2O ,
687 O_3 , and NO_2 by differential optical absorption, *J. Geophys. Res.*, 84(C10), 6329–6335,
688 10.1029/JC084iC10p06329, 1979.

689 Pyle, J. A., Zavody, A. M., Harries, J. E., and Moffat, P. H.: Derivation of OH concentration
690 from satellite infrared measurements of NO_2 and HNO_3 , *Nature*, 305, 690-692,
691 doi:10.1038/305690a0, 1983.

692 Pyle, J. A., and Zavody, A. M.: The derivation of hydrogen containing radical concentrations
693 from satellite data sets, *Q. J. R. Meteorol. Soc.*, 111, 993-1012, doi:10.1002/qj.49711147005,
694 1985.

695 Pickett, H. M., and Peterson, D. B.: Comparison of measured stratospheric OH with
696 prediction, *J. Geophys. Res.*, 101(D11), 16789–16796, doi: 10.1029/96JD01168, 1996.

697 Pickett, H. M., Drouin, B. J., Canty, T., Salawitch, R. J., Fuller, R. A., Perun, V. S., Livesey,
698 N. J., Waters, J. W., Stachnik, R. A., Sander, S. P., Traub, W. A., Jucks, K. W., and Minschwaner,
699 K.: Validation of Aura Microwave Limb Sounder OH and HO_2 measurements, *J. Geophys. Res.*,
700 113, D16S30, doi:10.1029/2007JD008775, 2008.

701 Rasch, P. J., Boville, B. A., and Brasseur, G. P.: A three-dimensional general circulation
702 model with coupled chemistry for the middle atmosphere, *J. Geophys. Res.*, 100(D5), 9041–9071,
703 doi: 10.1029/95JD00019, 1995.

704 Russell, J. P., and Lowe, R. P.: Atomic oxygen profiles (80–94 km) derived from Wind
705 Imaging Interferometer/Upper Atmospheric Research Satellite measurements of the hydroxyl

706 airglow: 1. Validation of technique, *J. Geophys. Res.*, 108, 4662, doi:10.1029/2003JD003454, D21,
707 2003.

708 Schwartz, M., Froidevaux, L., Livesey, N., and Read, W.: MLS/Aura Level 2 Ozone (O₃)
709 Mixing Ratio V004, Greenbelt, MD, USA, Goddard Earth Sciences Data and Information Services
710 Center (GES DISC), accessed 13.07.16, doi:10.5067/AURA/MLS/DATA2017, 2015.

711 Scinocca, J. F., McFarlane, N. A., Lazare, M., Li, J., Plummer, D.: The CCCma third
712 generation AGCM and its extension into the middle atmosphere, *Atmos. Chem. Phys.*, 8, 7055-
713 7074, doi:10.5194/acp-8-7055-2008, 2008.

714 Shimazaki, T.: *Minor Constituents in the Middle Atmosphere*, D. Reidel, Norwell, Mass.,
715 USA, 444 pp., 1985.

716 Siskind, D. E., Marsh, D. R., Mlynczak, M. G., Martin-Torres, F. J., and Russell III, J. M.:
717 Decreases in atomic hydrogen over the summer pole: Evidence for dehydration from polar
718 mesospheric clouds?, *Geophys. Res. Lett.*, 35, L13809, doi:10.1029/2008GL033742, 2008.

719 Siskind D. E., Mlynczak, M. G., Marshall, T., Friedrich, M., Gumbel, J.: Implications of odd
720 oxygen observations by the TIMED/SABER instrument for lower D region ionospheric modeling, *J.*
721 *Atmos. Sol. Terr. Phys.*, 124, 63–70, doi: 10.1016/j.jastp.2015.01.014, 2015.

722 Smith, A. K., Marsh, D. R., Mlynczak, M. G., and Mast, J. C.: Temporal variations of atomic
723 oxygen in the upper mesosphere from SABER, *J. Geophys. Res.*, 115, D18309,
724 doi:10.1029/2009JD013434, 2010.

725 Sobanski, N., Tang, M. J., Thieser, J., Schuster, G., Pöhler, D., Fischer, H., Song, W.,
726 Sauvage, C., Williams, J., Fachinger, J., Berkes, F., Hoor, P., Platt, U., Lelieveld, J., and Crowley,
727 J. N.: Chemical and meteorological influences on the lifetime of NO₃ at a semi-rural mountain site
728 during PARADE, *Atmos. Chem. Phys.*, 16, 4867-4883, doi:10.5194/acp-16-4867-2016, 2016.

729 Solomon, S., Rusch, D. W., Gerard, J.-C., Reid, G. C., and Crutzen, P. J.: The effect of
730 particle precipitation events on the neutral and ion chemistry of the middle atmosphere. 2. Odd
731 hydrogen, *Planet. Space Sci.*, 29, 885–892, 1981.

732 Solomon, P., Connor, B., Barrett, J., Mooney, T., Lee, A., and Parrish, A.: Measurements of
733 stratospheric ClO over Antarctica in 1996–2000 and implications for ClO dimer chemistry,
734 *Geophys. Res. Lett.*, 29(15), 1708, doi:10.1029/2002GL015232, 2002.

735 Sonnemann, G., Kremp, C., Ebel, A., and Berger, U.: A three-dimensional dynamic model of
736 minor constituents of the mesosphere, *Atmos. Environ.*, 32, 3157–3172, doi:10.1016/S1352-
737 2310(98)00113-7, 1998.

738 Sonnemann, G. R., Grygalashvyly, M., Hartogh, P., and Jarchow, C.: Behavior of
739 mesospheric ozone under nearly polar night conditions, *Adv. Space Res.*, 38, 2402–2407,
740 doi:10.1016/j.asr.2006.09.011, 2006.

741 Sonnemann, G. R., Hartogh, P., Jarchow, C., Grygalashvyly, M., and Berger, U.: On the
742 winter anomaly of the night-to-day ratio of ozone in the middle to upper mesosphere in middle to
743 high latitudes, *Adv. Space Res.*, 40, 846–854, doi:10.1016/j.asr.2007.01.039, 2007.

744 Sonnemann, G. R., Hartogh, P., Berger, U., and Grygalashvyly, M.: Hydroxyl layer: trend of
745 number density and intra-annual variability *Ann. Geophys.*, 33, 749–767, doi:10.5194/angeo-33-
746 749-2015, 2015.

747 Swenson, G. R., and Gardner, C. S.: Analytical models for the responses of the
748 mesospheric OH* and Na layers to atmospheric gravity waves, *J. Geophys. Res.*, 103(D6), 6271–
749 6294, doi:10.1029/97JD02985, 1998.

750 Stedman, D. H., Chameides, W., and Jackson, J. O.: Comparison of experimental and
751 computed values for J(NO₂), *Geophys. Res. Lett.*, 2(1), 22-25, doi:1029/GL002i001p00022, 1975.

752 Stimpfle, R. M., Wilmouth, D. M., Salawitch, R. J., and Anderson, J. G.: First measurements
753 of ClOOCl in the stratosphere: The coupling of ClOOCl and ClO in the Arctic polar vortex, *J.*
754 *Geophys. Res.*, 109, D03301, doi:10.1029/2003JD003811, 2004.

755 Sumińska-Ebersoldt, O., Lehmann, R., Wegner, T., Grooß, J.-U., Hösen, E., Weigel, R.,
756 Frey, W., Griessbach, S., Mitev, V., Emde, C., Volk, C. M., Borrmann, S., Rex, M., Stroh, F., and
757 von Hobe, M.: ClOOCl photolysis at high solar zenith angles: analysis of the RECONCILE self-
758 match flight, *Atmos. Chem. Phys.*, 12, 1353-1365, doi:10.5194/acp-12-1353-2012, 2012.

759 Thomas, R. J.: Atomic hydrogen and atomic oxygen density in the mesosphere region:
760 Global and seasonal variations deduced from Solar Mesosphere Explorer near-infrared emissions,
761 *J. Geophys. Res.*, 95, 16,457–16,476, doi:10.1029/JD095iD10p16457, 1990.

762 Tulet, P., Grini, A., Griffin, R. J., and Petitcol, S.: ORILAM-SOA: A computationally efficient
763 model for predicting secondary organic aerosols in three-dimensional atmospheric models, *J.*
764 *Geophys. Res.*, 111, D23208, doi:10.1029/2006JD007152, 2006.

765 von Hobe, M., Grooß, J.-U., Müller, R., Hrechanyy, S., Winkler, U., and Stroh, F.: A re-
766 evaluation of the ClO/Cl₂O₂ equilibrium constant based on stratospheric in-situ observations,
767 *Atmos. Chem. Phys.*, 5, 693-702, doi:10.5194/acp-5-693-2005, 2005.

768 von Hobe, M., Salawitch, R. J., Canty, T., Keller-Rudek, H., Moortgat, G. K., Grooß, J.-U.,
769 Müller, R., and Stroh, F.: Understanding the kinetics of the ClO dimer cycle, *Atmos. Chem. Phys.*,
770 7, 3055-3069, doi:10.5194/acp-7-3055-2007, 2007.

771 Walcek, C. J., and N. M. Aleksic, A simple but accurate mass conservative, peak preserving,
772 mixing ratio bounded advection algorithm with Fortran code, *Atmos. Environm.*, 32, 3863-3880,
773 1998.

774 Walcek, C. J., Minor flux adjustment near mixing ratio extremes for simplified yet highly
775 accurate monotonic calculation of tracer advection, *J. Geophys. Res.*, 105, 9335-9348, 2000.

776 Wang, S., Pickett, H., Livesey, N., and Read, W.: MLS/Aura Level 2 Hydroperoxy (HO₂)
777 Mixing Ratio V004, Greenbelt, MD, USA, Goddard Earth Sciences Data and Information Services
778 Center (GES DISC), accessed 13.07.16, doi:10.5067/AURA/MLS/DATA2013, 2015a.

779 Wang, S., Livesey, N., and Read, W.: MLS/Aura Level 2 Hydroxyl (OH) Mixing Ratio V004,
780 Greenbelt, MD, USA, Goddard Earth Sciences Data and Information Services Center (GES DISC),
781 accessed 13.07.16, doi:10.5067/AURA/MLS/DATA2018, 2015b.

782 Webster, C. R., May, R. D., Toumi, R., and Pyle, J. A.: Active nitrogen partitioning and the
783 nighttime formation of N₂O₅ in the stratosphere: Simultaneous in situ measurements of NO, NO₂,
784 HNO₃, O₃, and N₂O using the BLISS diode laser spectrometer, *J. Geophys. Res.*, 95(D9), 13851–
785 13866 doi: 10.1029/JD095iD09p13851, 1990.

786 Wetzel, G., Oelhaf, H., Kirner, O., Friedl-Vallon, F., Ruhnke, R., Ebersoldt, A., Kleinert, A.,
787 Maucher, G., Nordmeyer, H., and Orphal, J.: Diurnal variations of reactive chlorine and nitrogen
788 oxides observed by MIPAS-B inside the January 2010 Arctic vortex, *Atmos. Chem. Phys.*, 12,
789 6581-6592, doi:10.5194/acp-12-6581-2012, 2012.

790 Xu, J., Smith, A. K., Jiang, G., Gao, H., Wei, Y., Mlynczak, M. G., and Russell III, J. M.:
791 Strong longitudinal variations in the OH nightglow, *Geophys. Res. Lett.*, 37, L21801,
792 doi:10.1029/2010GL043972, 2010.

793 Xu, J., Gao, H., Smith, A. K., and Zhu, Y.: Using TIMED/SABER nightglow observations to
794 investigate hydroxyl emission mechanisms in the mesopause region, *J. Geophys. Res.*, 117,
795 D02301, doi:10.1029/2011JD016342, 2012.

797

798 **Table 1.** List of reactions with corresponding reaction rates from Burkholder et al. (2015).

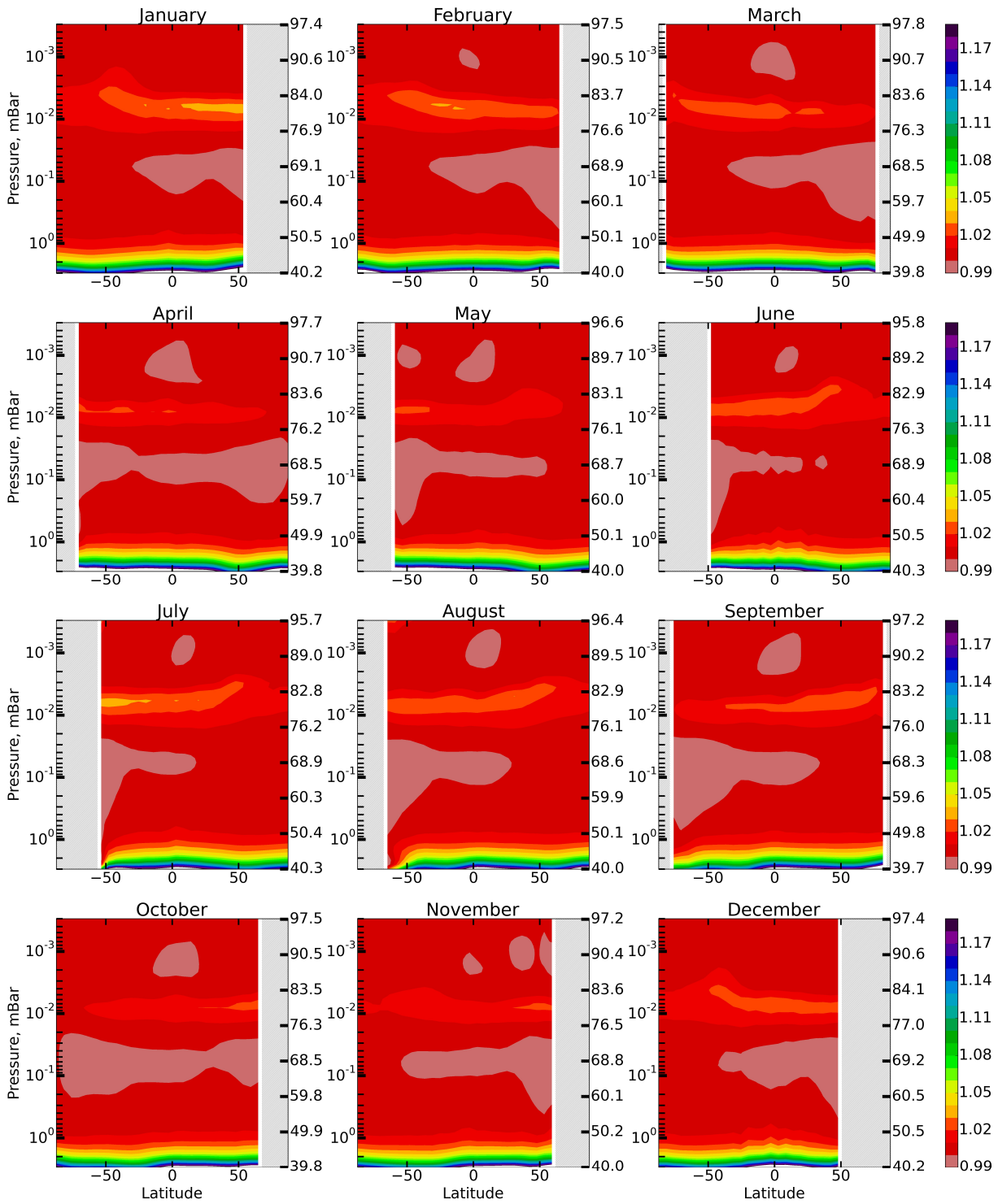
799

1	$O(^1D)+O_2 \rightarrow O+O_2$	22	$OH+O_3 \rightarrow O_2+HO_2$	43	$NO_2+O_3 \rightarrow NO_3+O_2$
2	$O(^1D)+N_2 \rightarrow O+N_2$	23	$HO_2+O_3 \rightarrow OH+2O_2$	44	$N+OH \rightarrow NO+H$
3	$O(^1D)+O_3 \rightarrow O_2+2O$	24	$H+OH+N_2 \rightarrow H_2O+N_2$	45	$NO+HO_2 \rightarrow NO_2+OH$
4	$O(^1D)+O_3 \rightarrow 2O_2$	25	$OH+H_2 \rightarrow H_2O+H$	46	$H+NO_2 \rightarrow OH+NO$
5	$O(^1D)+N_2O \rightarrow 2NO$	26	$OH+OH \rightarrow H_2O+O$	47	$NO_3+NO \rightarrow 2NO_2$
6	$O(^1D)+N_2O \rightarrow N_2+O_2$	27	$OH+OH+M \rightarrow H_2O_2+M$	48	$N+NO \rightarrow N_2+O$
7	$O(^1D)+H_2O \rightarrow 2OH$	28	$OH+HO_2 \rightarrow H_2O+O_2$	49	$N+NO_2 \rightarrow N_2O+O$
8	$O(^1D)+H_2 \rightarrow H+OH$	29	$H_2O_2+OH \rightarrow H_2O+HO_2$	50	$O_2+h\nu \rightarrow 2O$
9	$O(^1D)+CH_4 \rightarrow CH_3+OH$	30	$HO_2+HO_2 \rightarrow H_2O_2+O_2$	51	$O_2+h\nu \rightarrow O+O(^1D)$
10	$O(^1D)+CH_4 \rightarrow H_2+CH_2O$	31	$HO_2+HO_2+M \rightarrow H_2O_2+O_2+M$	52	$O_3+h\nu \rightarrow O_2+O$
11	$O+O+M \rightarrow O_2+M$	32	$CH_3+O \rightarrow CH_2O+H$	53	$O_3+h\nu \rightarrow O_2+O(^1D)$
12	$O+O_2+M \rightarrow O_3+M$	33	$OH+CO \rightarrow H+CO_2$	54	$N_2+h\nu \rightarrow 2N$
13	$O+O_3 \rightarrow O_2+O_2$	34	$CH_4+OH \rightarrow CH_3+H_2O$	55	$NO+h\nu \rightarrow N+O$
14	$H+HO_2 \rightarrow 2OH$	35	$CH_3+O_2+M \rightarrow CH_3O_2+M$	56	$NO_2+h\nu \rightarrow NO+O$
15	$H+HO_2 \rightarrow H_2O+O$	36	$O_3+N \rightarrow NO+O_2$	57	$N_2O+h\nu \rightarrow N_2+O(^1D)$
15	$H+HO_2 \rightarrow H_2+O_2$	37	$NO_3+O \rightarrow NO_2+O_2$	58	$N_2O+h\nu \rightarrow N+NO$
17	$OH+O \rightarrow H+O_2$	38	$O+NO+M \rightarrow NO_2+M$	59	$H_2O+h\nu \rightarrow H+OH$
18	$HO_2+O \rightarrow OH+O_2$	39	$NO_2+O \rightarrow NO+O_2$	60	$CH_4+h\nu \rightarrow CH_2+H_2$
19	$H_2O_2+O \rightarrow OH+HO_2$	40	$NO_2+O+M \rightarrow NO_3+M$	61	$H_2O_2+h\nu \rightarrow 2OH$
20	$H+O_2+M \rightarrow HO_2+M$	41	$N+O_2 \rightarrow NO+O$	62	$NO_3+h\nu \rightarrow NO_2+O$
21	$H+O_3 \rightarrow OH+O_2$	42	$NO+O_3 \rightarrow NO_2+O_2$	63	$CO_2+h\nu \rightarrow CO+O$

800

801

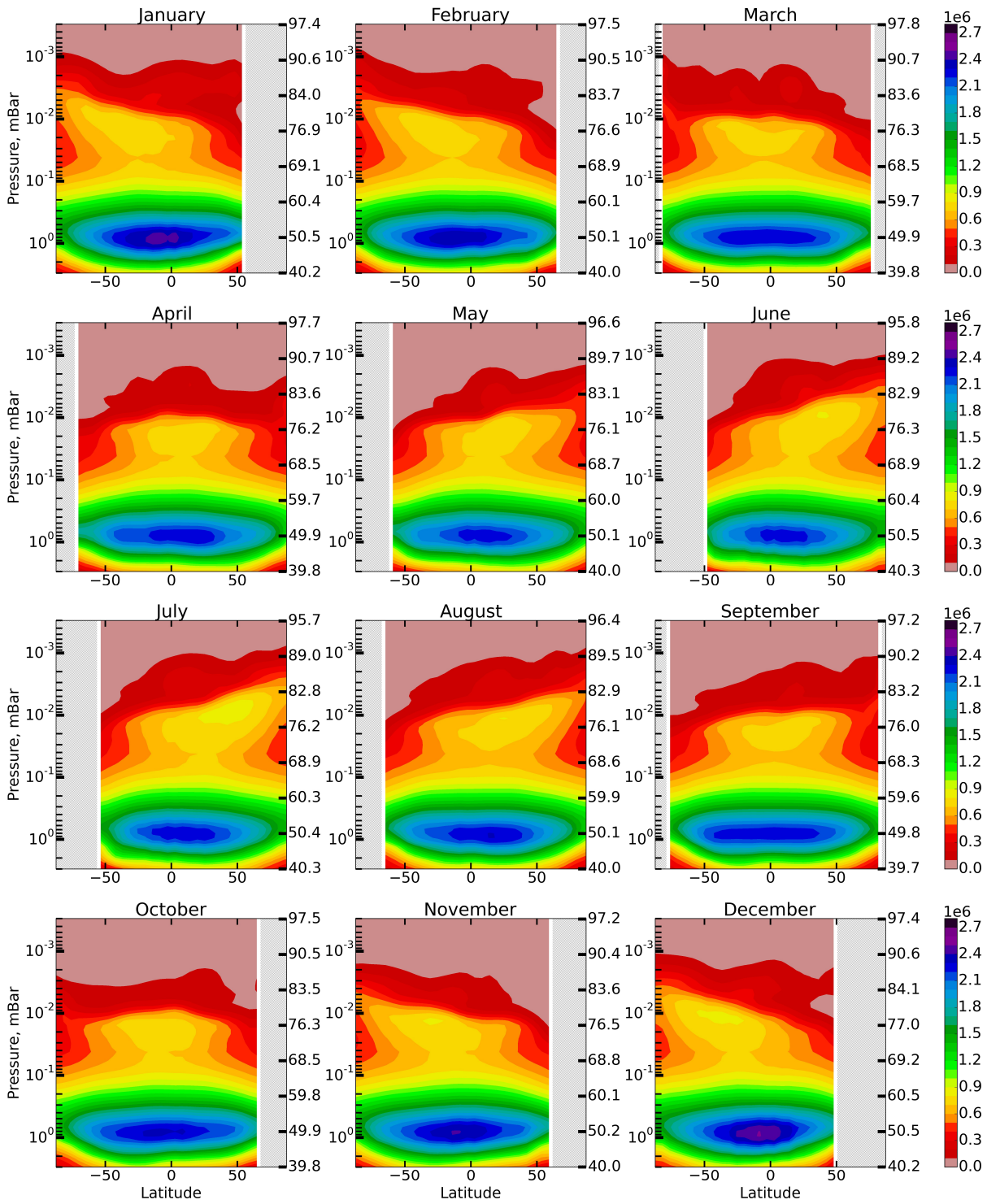
802



803

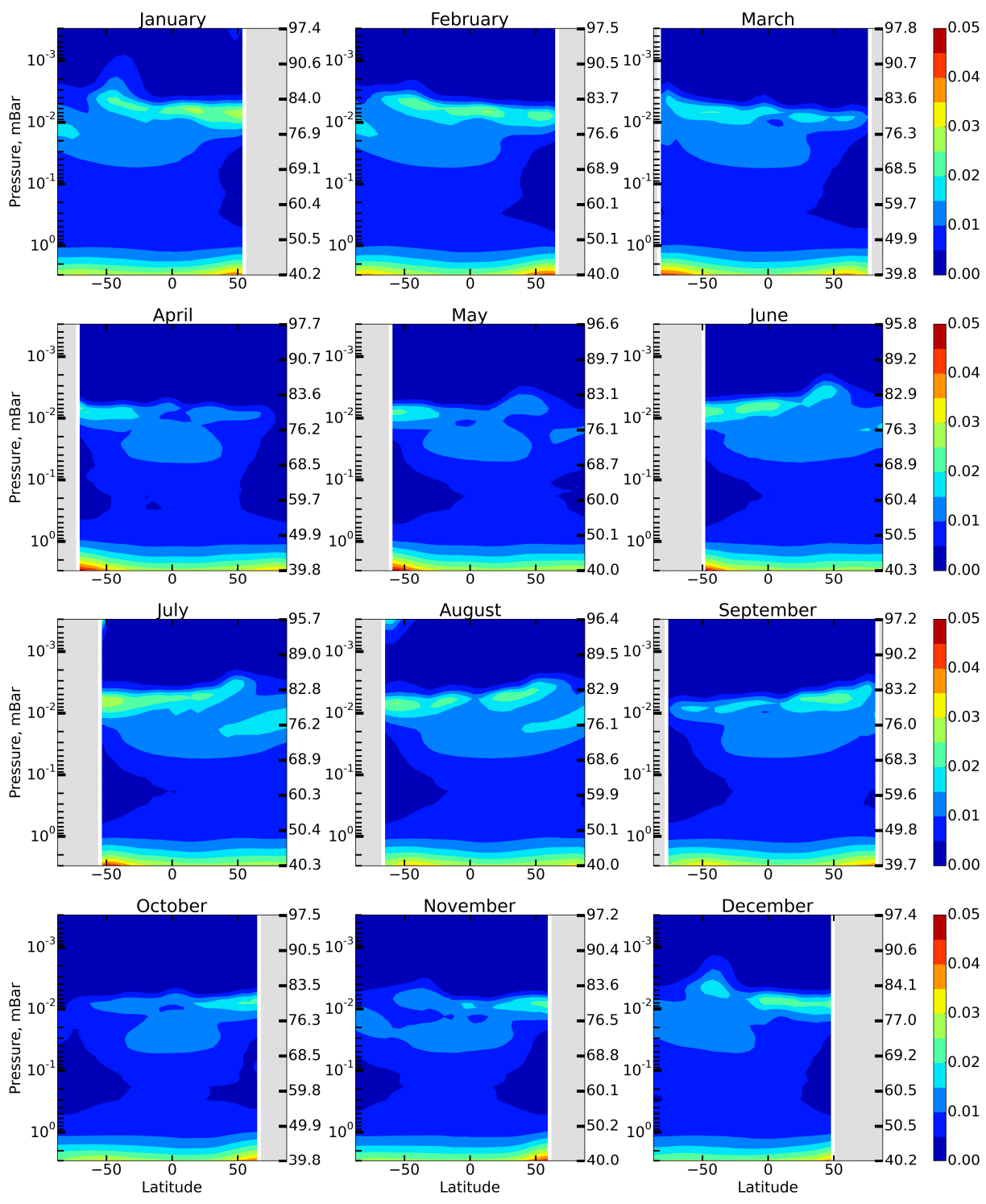
804 Figure 1. Daytime monthly averaged zonal mean F distributions.

805



808 Figure 2. Daytime monthly averaged zonal mean P_{OH} distributions (in $\text{cm}^{-3} \text{ s}^{-1}$).

810



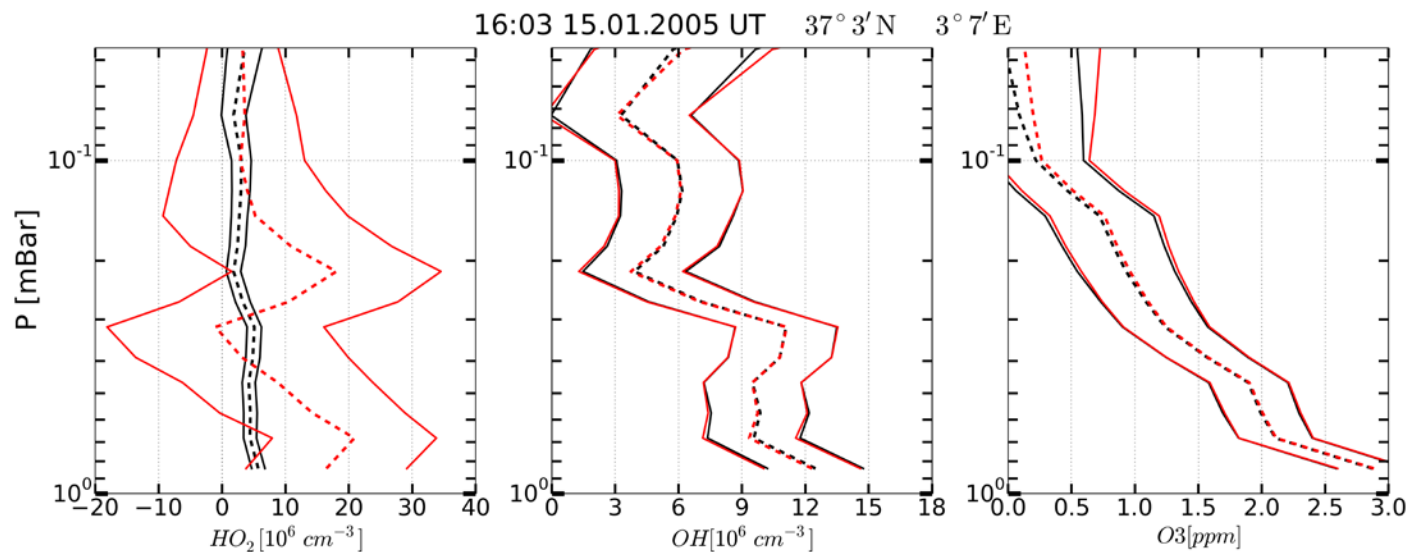
811

812

813 Figure 3. Daytime monthly averaged zonal mean $P_{OH}^{H_2O} / P_{OH}$ distributions.

814

815

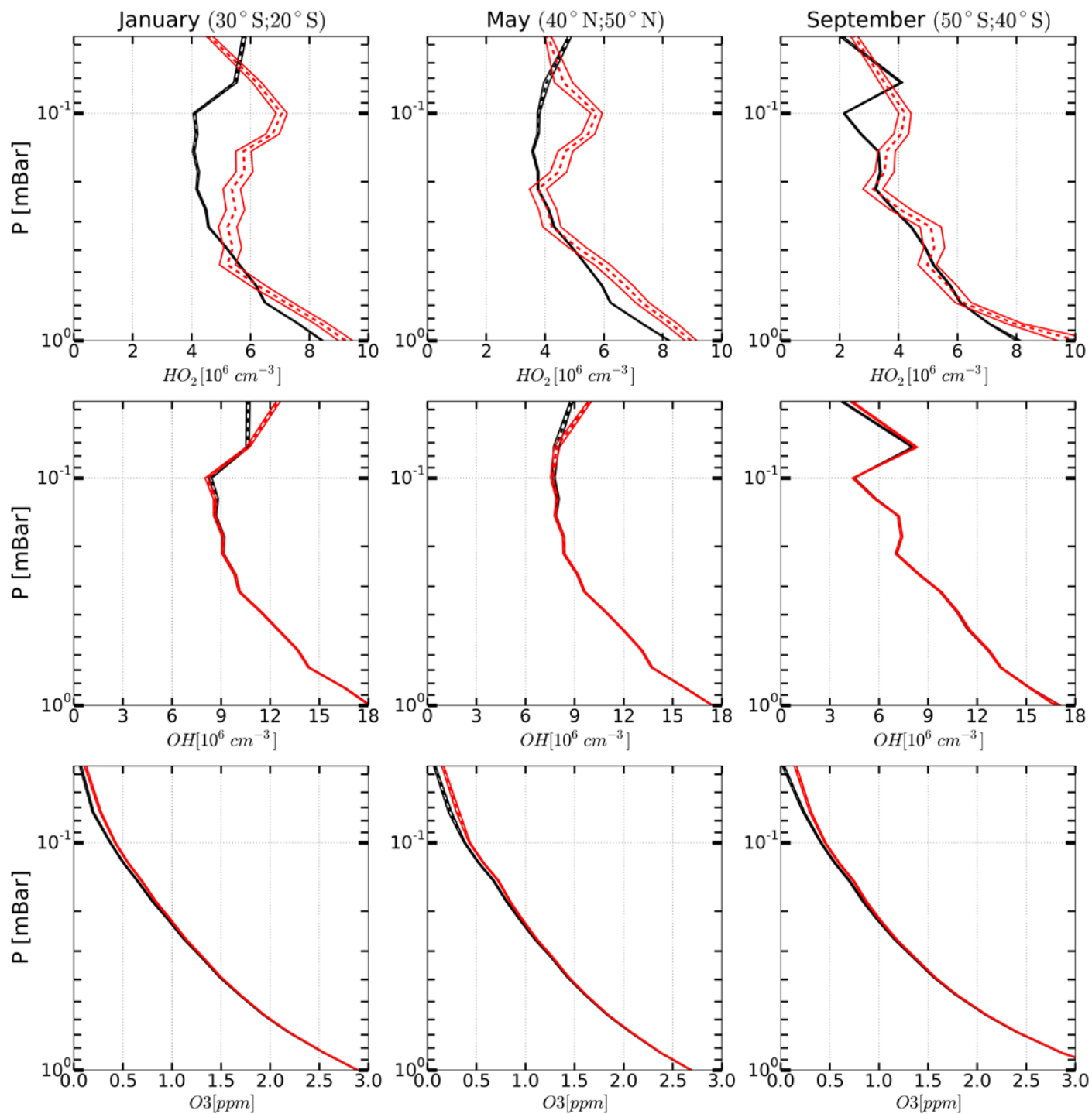


816

817

818 Figure 4. Example of OH, HO₂ and O₃ vertical profiles measured (red curves) on 15 January 2005
819 at 16.03 UT, 37°3'N, 3°7'E and corresponding retrieved profiles (black curves). Solid curves:
820 boundaries of the 65% confident intervals, dashed curves: medians.

821

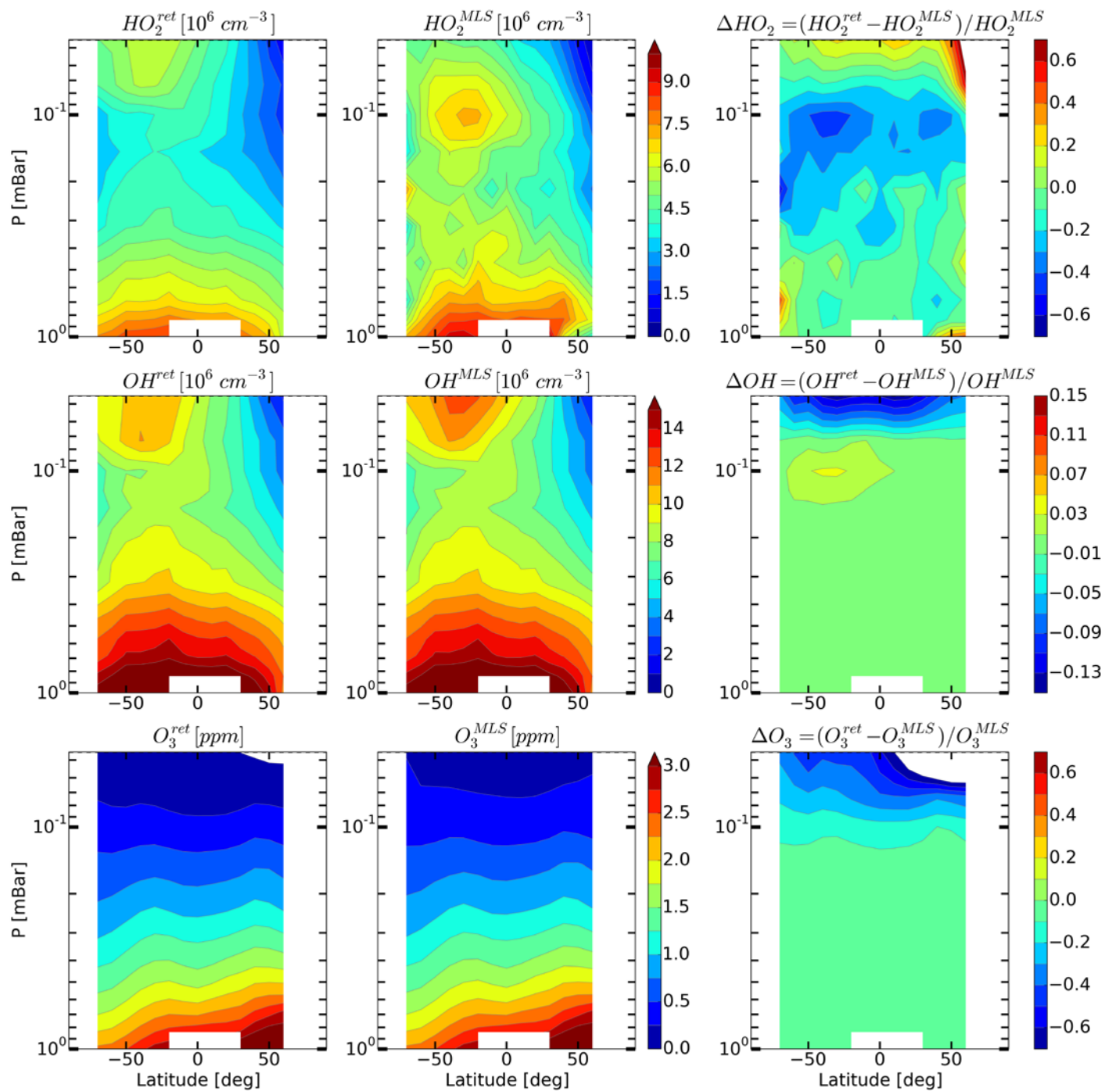


823

824

825 Figure 5. Examples of monthly averaged zonal mean vertical profiles of OH, HO₂ and O₃ measured
 826 (red curves) in January, May and March 2005 and corresponding retrieved profiles (black curves).

827 Solid curves: boundaries of the 65% confident intervals, dashed curves: medians.

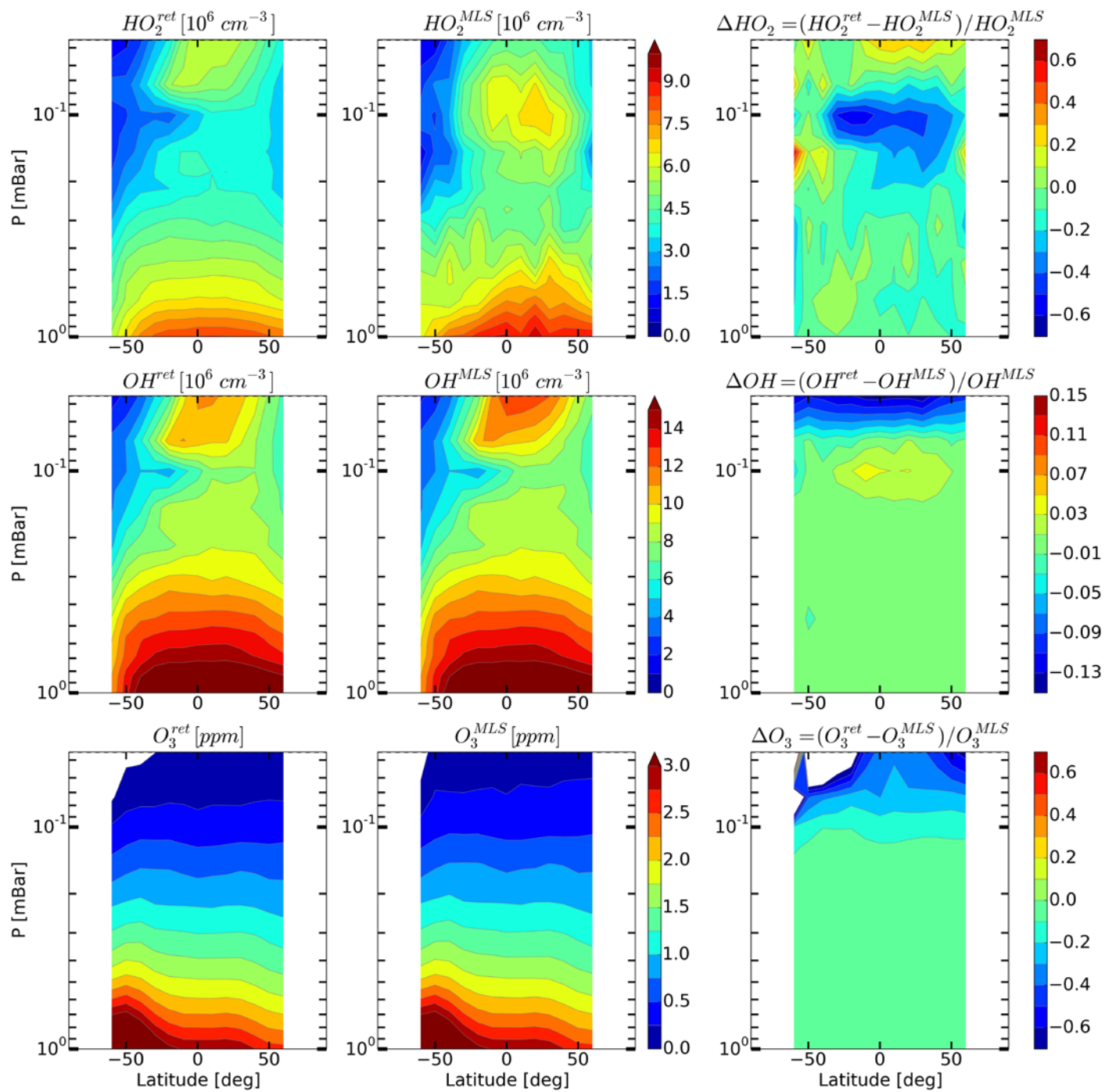


829

830

831 Figure 6. Daytime monthly averaged zonal mean retrieved (left column) and measured (middle
 832 column) distributions of HO_2 , OH , and O_3 and their relative difference (right column) in January
 833 2005.

834



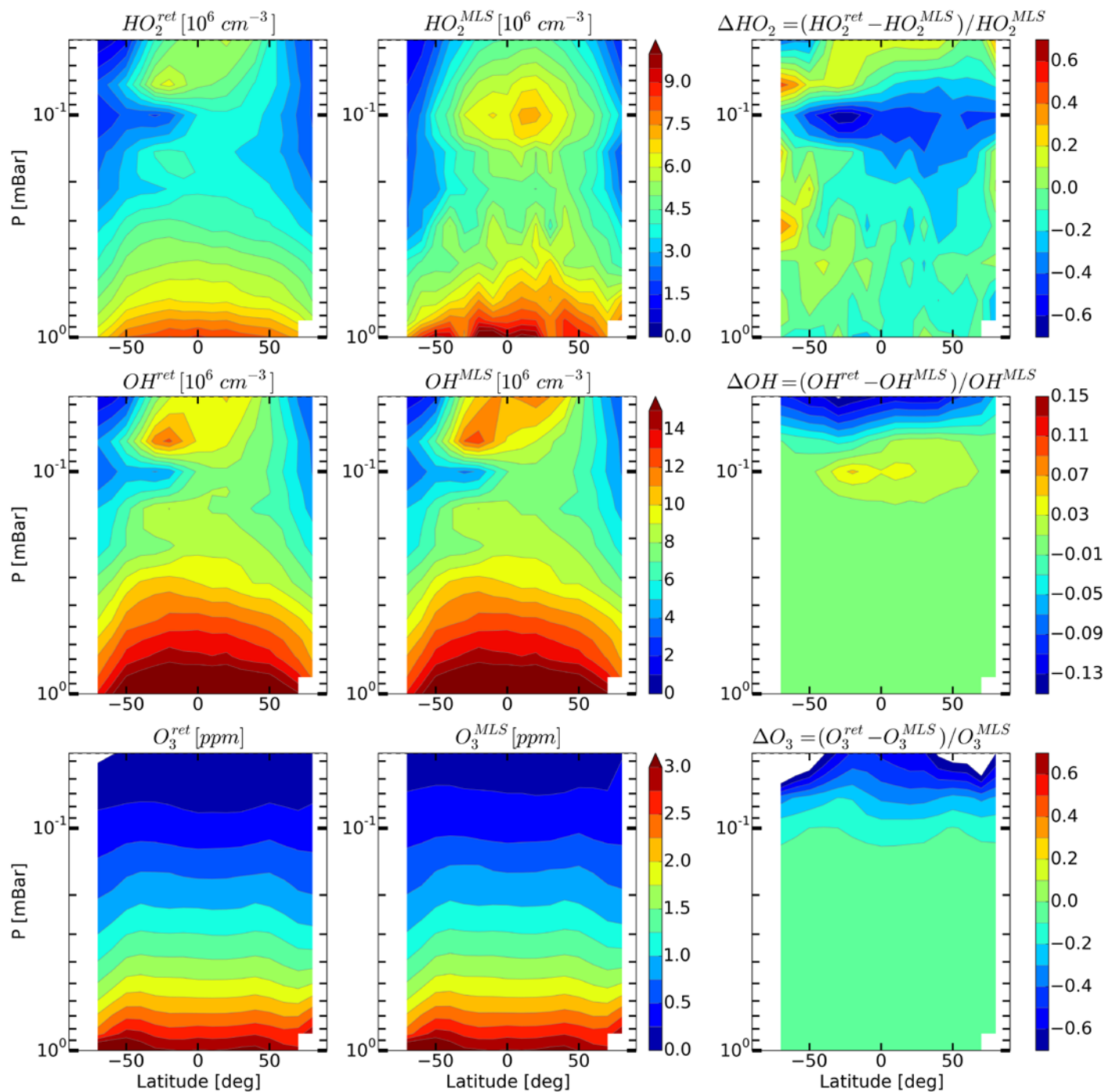
836

837

838 Figure 7. Daytime monthly averaged zonal mean retrieved (left column) and measured (middle
 839 column) distributions of HO_2 , OH , and O_3 and their relative difference (right column) for May 2005.

840

841

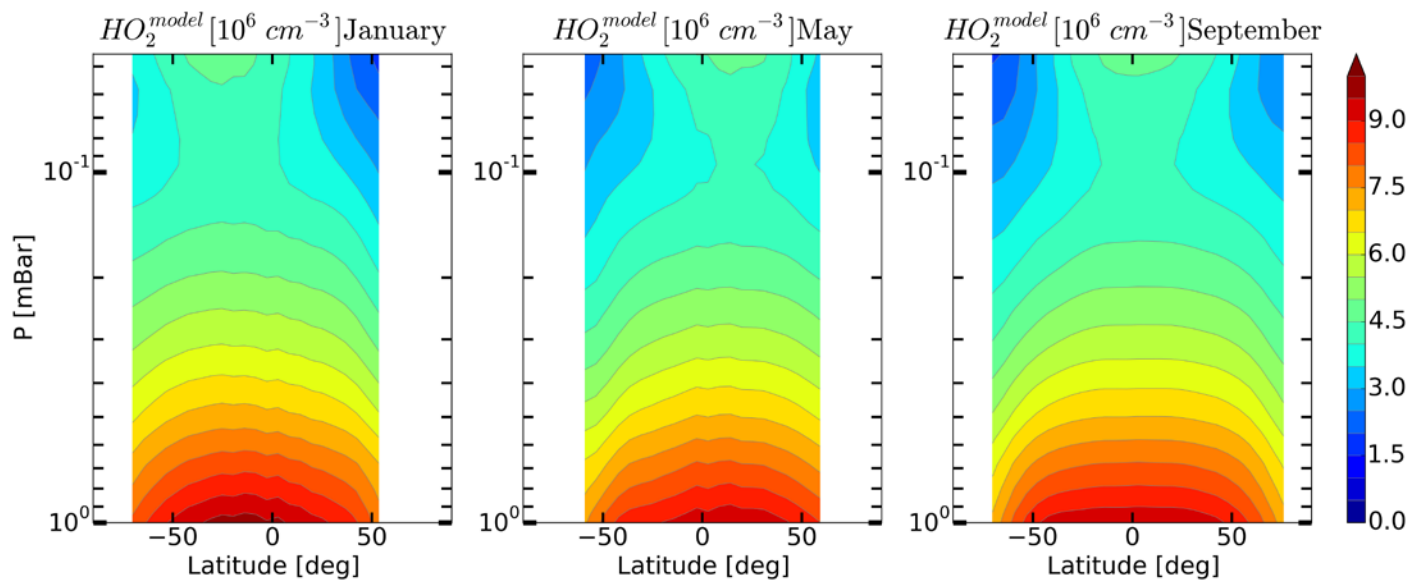


843

844

845 Figure 8. Daytime monthly averaged zonal mean retrieved (left column) and measured (middle
 846 column) distributions of HO_2 , OH , and O_3 and their relative difference (right column) for September
 847 2005.

848

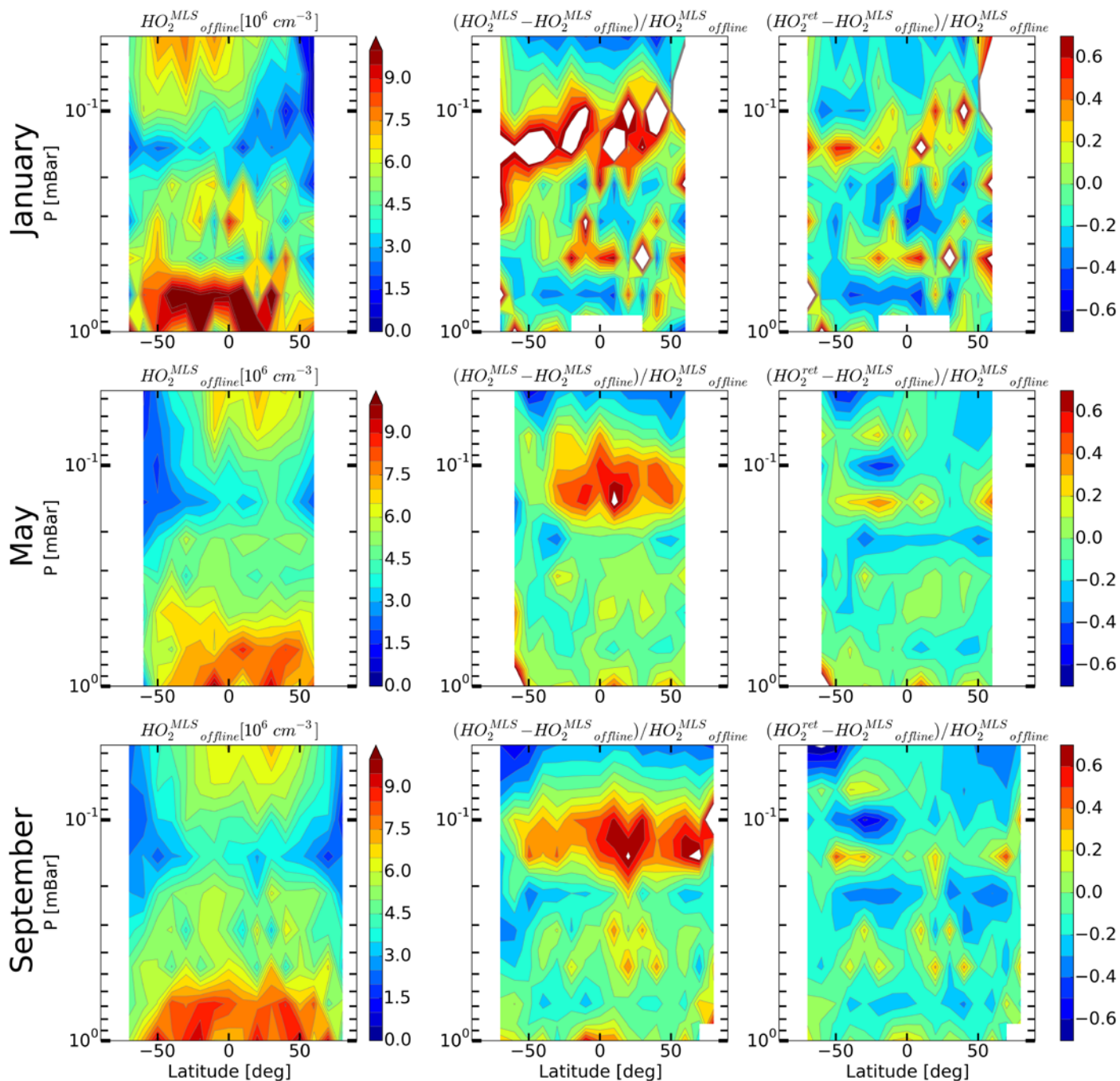


849

850 Figure 9. Daytime monthly averaged zonal mean model distributions of HO_2 for January, May, and
 851 September.

852

853



855

856

857 Figure 10. Daytime mean monthly averaged distributions of HO_2 retrieved by Millán et al. (2015)858 and relative differences $(\langle \text{HO}_2^{\text{MLS}} \rangle - \langle \text{HO}_2^{\text{MLS}_{\text{offline}}} \rangle) / \langle \text{HO}_2^{\text{MLS}_{\text{offline}}} \rangle$ and859 $(\langle \text{HO}_2^{\text{ret}} \rangle - \langle \text{HO}_2^{\text{MLS}_{\text{offline}}} \rangle) / \langle \text{HO}_2^{\text{MLS}_{\text{offline}}} \rangle$.